The transfer of a mitochondrial selfish element to the nuclear genome and its consequences

Julien Y. Dutheil[1,2,3,*], Karin Münch[2], Klaas Schotanus[2,4,5], Eva H. Stukenbrock[1,2,4], Regine Kahmann[2]

1. Max Planck Institute for Evolutionary Biology
August-Thienemann-Str. 2
24306 Plön, Germany

2. Max Planck Institute for Terrestrial Microbiology
Karl-von-Frisch-Str. 10
35043 Marburg, Germany

3. Institute of Evolutionary Sciences
CNRS - University of Montpellier – IRD - EPHE
Place Eugène Bataillon, 34095 Montpellier, France.

4. Christian Albrechts University of Kiel
24118 Kiel, Germany

5. Current address: Department of Molecular Genetics and Microbiology (MGM).
Duke University Medical Center. 213 Research Drive, 317 CARL Building, Box 3546 Durham, NC 27710 USA

Correspondence:
* Julien Y. Dutheil, dutheil@evolbio.mpg.de

Running head: Transfer of a mitochondrial homing endonuclease to the nuclear genome

Keywords: homing endonuclease, mitochondrion, intron, gene birth, gene transfer

Abstract

Homing endonucleases (HE) are enzymes capable of cutting DNA at highly specific target sequences, the repair of the generated double-strand break resulting in the insertion of the HE-encoding gene ("homing" mechanism). Some HE genes are found within Group I introns, where they further facilitate their excision and turn them into selfish invasive elements. HEs are present in all three domains of life and viruses; in eukaryotes, they are mostly found in the genomes of mitochondria and chloroplasts, as well as nuclear ribosomal RNAs. We here report the case of a HE that integrated into a telomeric region of the nuclear genome of the fungal maize pathogen *Ustilago maydis*. We show that the gene has a mitochondrial origin, but its original copy is absent from the *U. maydis* mitochondrial genome, suggesting a subsequent loss or a horizontal transfer. The telomeric HE underwent mutations in its active site and acquired a new start codon, but we did not detect significant transcription of the newly created open reading frame. The insertion site is located in a putative RecQ helicase gene, truncating the C-terminal domain of the protein. The truncated helicase is expressed during infection of the host, together with other homologous telomeric helicases. This unusual homing event represents a singular mutation leading to the creation of two new genes. The integrated HE gene subsequently lost its homing activity, while its insertion created a truncated version of an existing gene, possibly altering its function.

Introduction

The elucidation of the mechanisms at the origin of genetic variation is a longstanding goal of molecular evolutionary biology. Mutation accumulation experiments - together with comparative analysis of sequence data - are instrumental in studying the processes shaping genetic diversity at the molecular level (Kondrashov and Kondrashov 2010; Eyre-Walker and Keightley 2007). They revealed that the spectrum of mutations ranges from single nucleotide substitutions to large scale chromosomal rearrangements, and encompasses insertions, deletions, inversions, and duplication of genetic material of variable length (Lynch et al. 2008). Mutation events may result from intrinsic factors such as replication errors and repair of DNA damage. In some cases, however, mutations can be caused or favored by extrinsic factors, such as mutagenic environmental conditions or parasitic genome entities like viruses or selfish mobile elements. Such particular sequences, able to replicate and invade the host genome, may have various effects including inserting long stretches of DNA that do not encode any organismic function, but also disrupting, copying and moving parts of the genome sequence. These selfish element-mediated mutations can significantly contribute to the evolution of their host: first, the invasion of mobile elements creates “junk” DNA that can significantly increase the genome size (Lynch 2007), and some of this material can be ultimately domesticated and acquire a new function, beneficial to the host (Kaessmann 2010; Volff 2006). Second, the genome dynamics resulting from the activity of mobile elements can generate novelty by gene duplication (Ohta 2000; Dutheil et al. 2016) or serve as a mechanism of parasexuality and compensate for the reduced diversity in the absence of sexual reproduction (Dong et al. 2015; Möller and Stukenbrock 2017). Finally, control mechanisms (such as repeat-induced point mutations in fungi (Gladyshev 2017)) may also incidentally affect genetic diversity (Grandaubert et al. 2014).

Intron-borne homing endonuclease genes (HEG) constitute a class of selfish elements

56 whose impact on genome evolution is less well documented. They encode a protein able to
57 recognize a particular genomic DNA sequence and cut it (homing endonuclease, HE). The resulting
58 double-strand break is subsequently repaired by homologous recombination using the HEG itself as
59 a template, resulting in its insertion in the target location (Stoddard 2005). As the recognized
60 sequence is typically large, its occurrence is rare and the insertion typically happens at a
61 homologous position. In this process, a *heg*$^+$ element containing the endonuclease gene converts a
62 *heg*$^-$ allele (devoid of HEG but harbouring the recognition sequence) to *heg*$^+$, a mobility mechanism
63 referred to as *homing* (Dujon et al. 1989). After the insertion, the host cell is homozygous *heg*$^+$, and
64 the HEG segregates at a higher frequency than the Mendelian rate (Goddard and Burt 1999). The
65 open reading frame of the HEG is typically associated with a sequence capable of self-splicing,
66 either at the RNA (group-I introns) or protein (inteins) level, avoiding disruption of functionality
67 when inserted in a protein-coding gene (Chevalier and Stoddard 2001; Stoddard 2005). The
68 dynamic of HEGs has been well described, and involves three stages: (i) conversion from *heg*$^-$ to
69 *heg*$^+$ by homing activity, (ii) degeneration of the HEG leading to the loss of homing activity, but still
70 protecting against a new insertion because the target is altered by the insertion event and (iii) loss of
71 the HEG leading to the restoration of the *heg*$^-$ allele (Gogarten and Hilario 2006; Barzel et al. 2011).
72 This cycle leads to recurrent gains and losses of HEG at a given genomic position, and ultimately to
73 the loss of the HEG at the population level unless new genes invade from other locations or by
74 horizontal gene transfer (Gogarten and Hilario 2006).

75 HEGs are found in all domains of life as well as in the genomes of organelles,
76 mitochondria and chloroplasts (Stoddard 2005; Lambowitz and Belfort 1993; Belfort and Roberts
77 1997). In several fungi, HEGs are residents of mitochondria. Here, we study the molecular
78 evolution of a HEG from the fungus *Ustilago maydis*, which serves as a model for the elucidation
79 of (i) fundamental biological processes like cell polarity, morphogenesis, organellar targeting, and
80 (ii) the mechanisms allowing biotrophic fungi to colonize plants and cause disease (Steinberg and

81 Perez-Martin 2008; Djamei and Kahmann 2012; Ast et al. 2013). *U. maydis* is the most well-studied
82 representative of smut fungi, a large group of plant pathogens, because of the ease by which it can
83 be manipulated both genetically and through reverse genetics approaches (Vollmeister et al. 2012).
84 Besides, its compact, fully annotated genome comprises only 20.5 Mb and is mostly devoid of
85 repetitive DNA (Kämper et al. 2006). The genome sequences of several related species,
86 *Sporisorium reilianum*, *S. scitamineum,* and *U. hordei* causing head smut in corn, smut whip in
87 sugarcane and covered smut in barley, respectively, provide a powerful resource for comparative
88 studies (Schirawski et al. 2010; Laurie et al. 2012; Dutheil et al. 2016). Here, we report the case of a
89 mitochondrial HEG that integrated into the nuclear genome of *U. maydis*. This singular mutation
90 event created two new genes: first the original endonuclease activity of the integrated HEG was
91 inactivated by a deletion in the active site, leading to a frameshift and a new open reading frame
92 containing the DNA-binding domain of the HEG (Derbyshire et al. 1997). Second, the integration
93 of the HEG occurred within another protein-coding gene, leading to its truncation.

94 *Results*

95 We report the analysis of the nuclear gene *UMAG_11064* from the smut fungus *U.*
96 *maydis*, which was identified as an outlier in a whole-genome analysis of codon usage. We first
97 provide evidence that the gene is a former HEG and then reconstruct the molecular events that led
98 to its insertion in the nuclear genome using comparative sequence analysis. Finally, we assess the
99 phenotypic impact of the insertion event.

100 The *UMAG_11064* nuclear gene has a mitochondrial codon usage.

101 We studied the synonymous codon usage in protein-coding genes of the smut fungus *U.*
102 *maydis*, using within-group correspondence analysis. As opposed to other methods, within-group
103 correspondence analysis allows the comparison of codon usage while adequately taking into
104 account confounding factors such as variation in amino-acid usage (Perrière and Thioulouse 2002).

105 We report a distinct synonymous codon usage for nuclear genes and mitochondrial genes (Figure
106 1A), with the notable exception of the nuclear gene *UMAG_11064,* which displays a typical
107 mitochondrial codon usage. The *UMAG_11064* gene is located in the telomeric region of
108 chromosome 9, with no further downstream annotated gene (Figure 1B). It displays a low GC
109 content of 30%, which contrasts with the GC content of the flanking regions (50%) and the rather
110 homogeneous composition of the genome sequence of *U. maydis* as a whole. It is, however, in the
111 compositional range of the mitochondrial genome (Figure 1B). Altogether, the synonymous codon
112 usage and GC content of *UMAG_11064* suggest a mitochondrial origin.

113 In order to confirm the chromosomal location of *UMAG_11064*, we amplified and
114 sequenced three regions encompassing the gene using primers within the *UMAG_11064* gene and
115 primers in adjacent chromosomal genes upstream and downstream of *UMAG_11064* (Figure S1).
116 The sequences of the amplified segments were in full agreement with the genome sequence of *U.*
117 *maydis* (Kämper et al. 2006), thereby ruling out possible assembly artefacts in this region.
118 Surprisingly, the sequence of *UMAG_11064* has no match in the mitochondrial genome of *U.*
119 *maydis* (GenBank entry NC_008368.1), which suggests that *UMAG_11064* is an authentic nuclear
120 gene. As both the GC content and synonymous codon usage of *UMAG_11064* are indistinguishable
121 from the ones of mitochondrial genes and have not moved toward the nuclear equilibrium, the
122 transfer of the gene to its nuclear position is likely to have occurred relatively recently.

123 The *UMAG_11064* gene contains parts of a former GIY-YIG homing 124 endonuclease

125 To gain insight into the nature of the *UMAG_11064* gene, its predicted nucleotide
126 sequence was searched against the NCBI non-redundant nucleotide sequence database. High
127 similarity matches were found in the mitochondrial genome of three other smut fungi
128 (Supplementary Table S1): *S. reilianum* (87% nucleotide identity), *S. scitamineum* (79%), and *U.*

129 *bromivora* (76%). Two other very similar sequences were found in the mitochondrial genome of
130 two other smut fungi, *Tilletia indica* and *Tilletia walkeri* (69% nucleotide identity), as well as in
131 mitochondrial genomes from other basidiomycetes (e.g. *Laccaria bicolor*, 72%) and ascomycetes
132 (e.g. *Leptosphaeria maculans*, 69%, see Supplementary Table S1). The protein sequence of
133 *UMAG_11064* shows high similarity with fungal HEGs, in particular of the so-called GIY-YIG
134 family (Supplementary Table S2) (Stoddard 2005). The closest fully annotated protein sequence
135 matching *UMAG_11064* corresponds to the GIY-YIG HEG located in intron 1 of the *cox1* gene of
136 *Agaricus bisporus* (I-AbiIII-P). The amino-acid sequence of UMAG_11064 matches the N-terminal
137 part of this protein containing the DNA-binding domain of the HE (Derbyshire et al. 1997).

138 We performed a codon alignment of the *UMAG_11064* gene together with the most
139 similar sequences identified by Blast, using the Macse codon aligner to infer sequence alignment in
140 the presence of frameshifts (Ranwez et al. 2011). The sequences from *S. scitamineum* and *U.*
141 *bromivora* appeared to have several frameshifts introducing stop codons, suggesting that these
142 sequences are pseudogenes. We reconstructed the phylogeny of the nucleotide sequences after
143 removing ambiguously aligned regions (Figure 2). The resulting tree shows that the closest relative
144 of the *UMAG_11064* gene is the intronic sequence from *S. reilianum*.

145 As the GC profile of *UMAG_11064* suggests that the upstream region also has a
146 mitochondrial origin (Figure 1B), we performed a codon alignment of the 5' region with the full
147 intron sequences of S. *reilianum*, *T. indica* and *T. walkeri* as well as the sequence of I-AbIII-P from
148 *A. bisporus* in order to search for putative traces of the activity domain of the HE (Figure 3). We
149 found that the intergenic region between *UMAG_11065* and *UMAG_11064* is similar to the activity
150 domain of other GIY-YIG HE, and contains remnants of the former active site of the type GVY-
151 YIG (Figure 3). Compared to I-AbiIII-P and homologous sequences in *Tilletia*, however, a
152 frameshift mutation has occurred in the active site (a 7 bp deletion). The predicted gene model for
153 *UMAG_11064* starts at a conserved methionine position, 14 amino-acids downstream of the former

154 active site (Figure 3) and contains the *helix-turn-helix* DNA-binding domain of the original HE.

155 A branch model of codon sequence evolution was fitted to the codon sequence alignment
156 of *UMAG_11064* and its identified homologs, with the exception of the putative pseudogenes from
157 *S. scitamineum* and *U. bromivora*. The proteins appear to be evolving under purifying selection
158 (dN/dS < 1) on most branches of the tree, with the exception of the branches leading to the two
159 *Tilletia* sequences, as well as the branch leading to *UMAG_11064* (Figure 2). We note, however,
160 that the codeml program suffers from convergence issues on these particular branches, as witnessed
161 by the variance in final estimates after 10 independent runs (Figure 2). Such convergence failures
162 likely result from the branch model being an over-parametrized model, here fitted on relatively
163 short sequences. To further assess the possibility that the *UMAG_11064* gene is evolving under
164 positive selection, we fitted a branch-site model allowing specifically for sites in the *UMAG_11064*
165 gene to evolve under positive selection (foreground branch), which we contrasted with a null model
166 where all sites evolve under purifying selection or neutral evolution. The likelihood ratio test was
167 not significant (p-value equal to 0.1585), even after removing the *Tilletia* sequences (p-values equal
168 to 0.2183), and does not reject the hypothesis that the *UMAG_11064* gene is evolving under a
169 nearly neutral scenario. The higher dN/dS in the branch leading to *UMAG_11064* might, therefore,
170 be the result of relaxed purifying selection.

171 Altogether, these results suggest that *UMAG_11064* is a former HE that inserted into the
172 nuclear genome from the mitochondrion, was then inactivated by a deletion in its active site and
173 acquired a new start codon, allowing it to code for a protein sequence with the former nucleotide
174 binding domain of the HE.

175 The *UMAG_11064* gene is similar to an intronic mitochondrial sequence 176 of *S. reilianum*

177 The closest homologous sequence of *UMAG_11064* was found in the first intron of the

178 *cox1* gene of the smut fungus *S. reilianum* while this sequence was absent in the mitochondrial
179 genome of *U. maydis*. The *cox1* genes of *S. reilianum* and *U. maydis* both have eight introns, of
180 which only seven are homologous in position and sequence (Figure 4). *S. reilianum* has one extra
181 intron in position 1, while *U. maydis* has one extra intron in position 6. In *U. maydis* all introns but
182 the sixth one are reported to contain a HEG. A blast search of this intron's sequence, however,
183 revealed similarity with a homing endonuclease of type LAGLIDADG (Supplementary Table S4).
184 In *S. reilianum*, intron 1 (the putative precursor of *UMAG_11064)* and intron 2 are not annotated as
185 containing a HEG. Blast searches of the corresponding sequences, however, provided evidence for
186 homology with a GIY-YIG HE (Supplementary Table S5) and a LAGLIDADG HE, respectively
187 (Supplementary Table S6). Like many other species of fungi (Stone et al. 2018; Jalalzadeh et al.
188 2015; Pogoda et al. 2019), plants (Cho et al. 1998) and even animals (Fukami et al. 2007; Schuster
189 et al. 2017), the *cox1* gene seems to be a hotspot of Group I introns in smut fungi.

190 Lastly, intron 1 in *S. reilianum* was not detected in *U. maydis*. A closer inspection showed
191 that the ORF could be aligned with related HEs (Figure 3). This alignment revealed an insertion of
192 four amino-acids, a deletion of the first glycine residue in the active site plus several frameshifts at
193 the beginning of the gene, which suggests that this gene has been altered and might not encode a
194 functional HE any longer.

195 *UMAG_11064* inserted into a gene encoding a RecQ helicase

196 In order to study the effect of the HEG insertion in the nuclear genome, we looked at the
197 genomic environment of the *UMAG_11064* gene. Downstream of *UMAG_11064* are telomeric
198 repeats, while the next upstream gene, *UMAG_11065*, is uncharacterized. A similarity search for
199 *UMAG_11065* detected 13 homologous sequences in the *U. maydis* genome (including one,
200 *UMAG_12076*, on an unmapped contig), but only low-similarity matches in other sequenced smut
201 fungi (see Methods). The closest non-smut related sequence comes from a gene from *Fusarium*
202 *oxysporum*. We inferred the evolutionary relationships between the 14 genes by reconstructing a

203 maximum likelihood phylogenetic tree, and found that the *UMAG_11065* gene is closely related to
204 *UMAG_04486*, located on chromosome 14 (Figure 5 and Table 1). The *UMAG_04486* gene,
205 however, is predicted to be almost six times as long as *UMAG_11065*. We note that the downstream
206 region of *UMAG_11064* does not show any similarity with the 3' part of the *UMAG_04486* gene,
207 suggesting that the insertion of the HEG did not lead to the formation of an intron in the
208 *UMAG_11065* gene, but rather to its truncation. A search for similar sequences of *UMAG_11065*
209 and its relatives in public databases revealed homology with so-called RecQ helicases
210 (Supplementary Table S3), enzymes known to be involved in DNA repair and telomere expansion
211 (Singh et al. 2012). While this function is only predicted by homology, we note that all 12
212 chromosomal *recQ* related genes are located very close to telomeres in *U. maydis* (Table 1),
213 suggesting a role of these gene in telomere maintenance (Sánchez-Alonso and Guzmán 1998).
214 Lastly, we tested whether the truncation of *UMAG_11065* was followed by positively selected
215 mutations in the remaining part of the gene. Our results suggested, however, that the *UMAG_11065*
216 gene evolved under purifying selection (dN/dS ratio equal to 0.342).

217 *U. maydis* populations shows structural polymorphism in the telomeric 218 region of chromosome 9

219 Because the *UMAG_11064* gene still displays a strong signature of its mitochondrial
220 origin (codon usage and GC content), its transfer may have occurred recently. In order to provide a
221 timeframe for the insertion event, we examined the structure of the genomic region of the insertion
222 in other *U. maydis* and *S. reilianum* isolates, as well as the structure of the *cox1* exons 1, 2 and 7.
223 The regions that could be amplified and their corresponding sizes are listed in Supplementary
224 Figure S2 and the inferred genome organisations are summarized in Figure 6. The *UMAG_11064*
225 gene is present in the FB1-derived strain SG200, as well as in the Holliday strains 518 and 521, but
226 is absent in the nuclear and mitochondrial genome sequences of a recent *U. maydis* isolate from the

227 US, strain 10-1, as well as from 5 Mexican isolates (I2, O2, P2, S5 and T6, Figure S2A).
228 Conversely, the *UMAG_11072* gene, which is located further away from the telomere on the same
229 chromosome arm, could be amplified in all strains. This positive control demonstrates that the lack
230 of amplification of *UMAG_11064* in some strains is not due to any issue with the quality of the
231 extracted DNA (Figure S2B). These results suggest that, either the *UMAG_11064* gene was
232 ancestral to all tested strains and subsequently lost in the Mexican and 10-1 strains, or it inserted in
233 an ancestor of the two strains 518 and 521, after the divergence from other *U. maydis* strains, an
234 event that occurred after the domestication of maize and the spread of the associated pathogen,
235 10,000 to 6,000 years ago (Munkacsi et al. 2008). Moreover, all *U. maydis* strains possess intron 6
236 in the mitochondrial *cox1* gene, which is absent in *S. reilianum*. While the three *S. reilianum* strains
237 tested carry intron 1, the most direct descendant of the progenitor of the HEs, it was absent in all *U.*
238 *maydis* strains tested (Figure S2C-E and Figure 6).

239 Functional characterization

240 To shed light on the functional implication of the translocation of the HEG and
241 subsequent mutations we (i) assessed the expression profile of these genes and (ii) generated a
242 deletion strain and phenotyped it. For the expression analysis we relied on a previously published
243 RNASeq data set (Lanver et al. 2018), from which we extracted the expression profiles of genes in
244 the telomeric region of chromosome 9 (Figure 7A). While the expression of *UMAG_11064*
245 remained close to zero in the three replicates, expression of *UMAG_11065* increased during plant
246 infection. The telomeric region was highly heterogeneous in terms of expression profile: while
247 *UMAG_11066* and *UMAG_03393* did not show any significant level of expression, *UMAG_03392*
248 was down-regulated at twelve hours post-infection, while *UMAG_03394*, another RecQ-encoding
249 gene homologous to *UMAG_11065,* displayed constitutively high levels of expression (Figure 7A).
250 All homologs of *UMAG_11065* show a significantly higher expression during infection (Tukey's
251 posthoc test, false discovery rate of 5%, Figure 7B). The comparison of expression profiles revealed

252 two main classes of genes (Figure 7C): highly expressed genes (upper group), and moderately
253 expressed genes (lower group), to which *UMAG_11065* belongs. We further note that the
254 differences in expression profiles do not mirror the protein sequence similarity of the genes (Mantel
255 permutation test, p-value = 0.566).

256 To assess the functional role of *UMAG_11064* and *UMAG_11065*, these genes were
257 simultaneously deleted in SG200, a solopathogenic haploid strain that can cause disease without a
258 mating partner (Kämper et al. 2006) using a single-step gene replacement method (Kämper 2004).
259 Gene deletion was verified by Southern analysis (Figure S3). Virulence assays, conducted in
260 triplicate revealed no statistically different symptoms of the double deletion strain,
261 SG200Δ11065Δ11064, compared to SG200 in infected maize plants (Figure 8A, Chi-square test, p-
262 value = 0.453). Since RecQ helicases contribute to dealing with replication stress (Kojic and
263 Holloman 2012) we also determined the sensitivity of the mutant to various stressors including UV,
264 hydroxyurea and Congo Red. (Figure 8B). We report that the deletion strain shows increased
265 sensitivity to cell wall stress induced by Congo Red and increased resistance to UV stress. Since
266 *UMAG_11064* does not show any detectable level of expression, we hypothesize that the deletion of
267 *UMAG_11065* is responsible for this phenotype.

268 Discussion

269 The codon usage and GC content of the *UMAG_11064* gene, as well as its similarity to
270 known mitochondrial HEGs, points at a recent transfer into the nuclear genome of *U. maydis*.
271 Moreover, the precursor of this gene is absent from the mitochondrial genome of this species. Two
272 possible scenarios can explain this pattern, which we detail below.

273 The first scenario involves a transfer of the gene to the nuclear genome followed by a loss
274 of the mitochondrial copy (Figure 9). Under this scenario, the mitochondrial HEG was present in
275 the *U. maydis* ancestor. Two evolutionary events are invoked: the insertion of the HEG into the

276 nuclear genome, on the one hand, creating a HEG^+ genotype at the nuclear locus (designated
277 $[HEG^+]_{nuc}$), and the loss of the mitochondrial copy, creating a HEG^- genotype at the mitochondrial
278 locus (designated $[HEG^-]_{mit}$). These two events may have happened at distinct time points, but,
279 under this scenario, the former cannot have happened after the fixation of the $[HEG^-]_{mit}$ genotype in
280 the population. The $[HEG^+]_{nuc}$ / $[HEG^-]_{mit}$ genotype could be generated by a cross between two
281 individuals, one $[HEG^+]_{nuc}$ and the other $[HEG^-]_{mit}$, given that mitochondria are uniparentally
282 inherited in *U. maydis* (Basse 2010). Importantly, the segregation of the $[HEG^+]_{nuc}$ and $[HEG^-]_{mit}$
283 variants could be purely neutral and driven by genetic drift only. In case the $[HEG^-]_{nuc}$ allele
284 contained a recognition sequence of the HE, the $[HEG^+]_{nuc}$ allele may have initially benefited from a
285 genetic drive effect. Any putative selective advantage/disadvantage of the $[HEG^+]_{nuc}$ or $[HEG^-]_{mit}$
286 alleles may have favored their fixation, or on the contrary, acted against it.

287 In the second scenario, the mitochondrial HEG was not ancestral to *U. maydis*, but was
288 horizontally transferred from *S. reilianum* (or a related species). The high similarity of the
289 *UMAG_11064* gene to the *S. reilianum* mitochondrial HEG (Figure 3) supports this hypothesis,
290 given the relatively high nucleotide divergence between the two species, which diverged around 20
291 My ago (Schweizer et al. 2018). We note, however, that intronic HEGs have also been reported to
292 show reduced nucleotide substitution rates, which can potentially explain their comparatively low
293 divergence (Jalalzadeh et al. 2015). Group I introns have been reported to be highly mobile and to
294 undergo frequent horizontal gene transfers (HGT) within metazoans (Schuster et al. 2017), plants
295 (Sanchez-Puerta et al. 2008) and fungi (Jalalzadeh et al. 2015; Férandon et al. 2010). Group I
296 introns in metazoans and plants are also thought to originate from a fungal donor (Schuster et al.
297 2017; Sanchez-Puerta et al. 2008, 2011). In this respect, a transfer from another *cox1* intron-
298 carrying smut fungus to *U. maydis* is not unlikely, given that *U. maydis* and *S. reilianum* share the
299 same host, and that hybridization between smut species has been reported (Fischer 1957; Boidin
300 1986).

301 We further note that the phylogeny of *UMAG_11064* with the *cox1* introns 1 (Figure 2)
302 mirrors the phylogeny of the corresponding species of smut fungi (Schweizer et al. 2018), notably
303 grouping the *S. scitamineum cox1* intronic sequence with that of *S. reilianum*, despite a long branch
304 and the presence of multiple frameshifts. If confirmed, this phylogeny would, therefore, suggest the
305 existence of a homologous HEG-containing intron in the ancestral *U. maydis* strain, or that the
306 horizontal transfer predated the split between *S. reilianum* and *S. scitamineum*, thought to have
307 occurred 13 My ago.

308 HEGs are found in eukaryotic nuclei but are usually restricted to small and large
309 ribosomal RNA subunit genes (Lambowitz and Belfort 1993; Dunin-Horkawicz et al. 2006). While
310 transfer of DNA segments and functional genes from organellar genomes to the nucleus is well
311 documented (Sun and Callis 1993; Thorsness and Weber 1996; Lloyd and Timmis 2011; Fuentes et
312 al. 2012), established examples of HEG insertions at other genomic locations than rRNA genes is
313 very scarce. Louis and Haber (Louis and Haber 1991) reported such a transfer into a telomeric
314 region of *Saccharomyces cerevisiae*. The authors argue that signatures of such insertion could be
315 found because (i) it had no deleterious effect and (ii) the occurrence of heterologous recombination
316 between telomeres favours the maintenance of elements that would otherwise be lost. Contrasting
317 with this result, the insertion of the GIY-YIG HEG that inserted into the ancestor of the
318 *UMAG_11065* gene potentially had non-neutral effects, resulting in an expressed truncated protein.
319 Several mutations were found within the active site of the inserted HEG that led to the
320 *UMAG_11064* gene, suggesting that the encoded protein is unlikely to act as a HE any longer.
321 However, an alternative start codon was detected, downstream the active site, followed by an
322 uninterrupted peptide sequence containing the helix-turn-helix binding domain of the original HE.
323 While we cannot rule out that the UMAG_11064 protein acquired a new, yet unknown, function, we
324 could not detect any significant level of expression of the *UMAG_11064* gene in various laboratory
325 conditions. Comparative sequence analysis further suggests that *UMAG_11064* is evolving under

326 relaxed purifying selection, indicating that it might be undergoing pseudogenization. However, as
327 this mitochondrial HEG inserted into a nuclear *U. maydis* gene, it might have had phenotypic
328 consequences not directly due to the HEG gene itself. The *UMAG_11065* gene appeared truncated
329 by the HEG insertion, which removed the C-terminal part of the encoded protein, a likely RecQ
330 helicase, and the truncated *UMAG_11065* is expressed during infection. The truncation likely did
331 not have a strong negative impact, possibly because of the existence of multiple potentially
332 functionally redundant paralogs of *UMAG_11065,* including on the same telomeric region of
333 chromosome 9, with *UMAG_03394* being located 4 genes upstream (Table 1). While we were
334 unable to detect a contribution to virulence, our results point at a putative role of the truncated RecQ
335 helicase into stress tolerance, as its deletion increases resistance to UV radiation but makes the
336 fungus more susceptible to cell wall stress, at least under laboratory conditions. How the truncated
337 UMAG_11065 RecQ helicase could improve coping with cell wall stress and increases the
338 sensitivity to UV simultaneously, however, remains to be investigated, as well as the potential
339 fitness benefit or cost of these phenotypes.

340 *Conclusions*

341 In this study, we report instances of two stages of the life cycle of HEGs. Intron 1 of the
342 mitochondrial *cox1* gene of *S. reilianum* was shown to contain a degenerated GIY-YIG HEG, while
343 the homologous position in the *U. maydis* gene displays no intron. Besides, in the telomeric region
344 of chromosome 9 of the nuclear genome of *U. maydis*, we found evidence of a recent insertion of a
345 very similar GIY-YIG HEG. Phenotypic assay of the mutant strain containing a double-deletion of
346 the HEG and the helicase gene where it inserted reveals enhanced stress sensitivity *in vitro*. The
347 absence of a GIY-YIG HEG in any field isolates of *U. maydis* sequenced so far, however, suggests
348 that either the mutation was lost in natural populations and only maintained under laboratory
349 conditions, or that it is only present in a so far unsampled population. These results demonstrate that

350 HEGs can generate genetic diversity not only via their duplication, but also by drastically
351 modifying the local genetic architecture where they insert.

352 *Material and Methods*

353 Data sets and scripts necessary to reproduce the statistical analyses in this work are
354 available as Supplementary File S1 and at https://gitlab.gwdg.de/molsysevol/umag_11064 .
355

356 Analysis of codon usage and GC content

357 *Ustilago maydis* gene models (genome version 2.0) were retrieved from the MIPS
358 database (Mewes et al. 2011). Mitochondrial genes were extracted from the *U. maydis* full
359 mitochondrial genome (Genbank accession number: NC_008368.1). Within-group correspondence
360 analysis of synonymous codon usage was performed using the ade4 package for R, following the
361 procedure described in (Charif et al. 2005). The proportion of G and C nucleotides was computed
362 along with the first 10 kb of *U. maydis* chromosome 9, using 300 bp windows slid by 1 bp. The
363 corresponding R code is available as Supplementary File S1.

364 Strains, growth conditions and virulence assays

365 The *Escherichia coli* strains DH5α (Bethesda Research Laboratories) and TOP10 (Life
366 Technologies, Carlsbad, CA, USA) were used for the cloning and amplification of plasmids. *U.*
367 *maydis* strains 518 and 521 are the parents of FB1 and FB2 (Banuett and Herskowitz 1989). SG200
368 is a hapoid solopathogenic strain derived from FB1 (Kämper et al. 2006). 10-1 is an uncharacterized
369 haploid *U. maydis* strain isolated in the US and kindly provided by G. May. I2, O2, P2, S5, and T6
370 are haploid *U. maydis* strains collected in different parts of Mexico (Valverde et al. 2000). The
371 haploid *S. reilianum* strains SRZ1 and SRZ2 as well as the solopathogenic strain JS161 derived

372 from SRZ1 have been described (Schirawski et al. 2010). Deletion mutants were generated by gene
373 replacement using a PCR-based approach and verified by Southern analysis (Kämper 2004).
374 pRS426Δum11064+11065 is a pRS426-derived plasmid containing the *UMAG_11064*/
375 *UMAG_11065* double deletion construct which consists of a hygromycin resistance cassette flanked
376 by the left border of the *UMAG_11064* and right border of the *UMAG_11065* gene. The left border
377 of *UMAG_11064* and the right border of *UMAG_11065* were PCR amplified from SG200 gDNA
378 with primers um11064_lb_fw/um11064_lb_rv and um11065_rb_fw/um11065_rb_rv
379 (Supplementary Table S7). The hygromycin resistance cassette was obtained from SfiI digested
380 pHwtFRT (Khrunyk et al. 2010). The pRS426 EcoRI/XhoI backbone, both borders and the
381 resistance cassette were assembled using yeast drag and drop cloning (Christianson et al. 1992). The
382 fragment containing the deletion cassette was amplified from this plasmid using primers
383 um11064_lb_fw and um11065_rb_rv (Supplementary Table S7), transformed into SG200 and
384 transformants carrying a deletion of *UMAG_11064* and *UMAG_11065* were identified by southern
385 analysis (Figure S3).
386 *U. maydis* strains were grown at 28°C in liquid YEPSL medium (0.4% yeast extract, 0.4%
387 peptone, 2% sucrose) or on PD solid medium (2.4% Potato Dextrose broth, 2% agar). Stress assays
388 were performed as described in (Krombach et al. 2018). Transformation and selection of *U. maydis*
389 transformants followed published procedures (Kämper et al. 2006). To assess virulence, seven day
390 old maize seedlings of the maize variety Early Golden Bantam (Urban Farmer, Westfield, Indiana,
391 USA) were syringe-infected. At least three independent infections were carried out and disease
392 symptoms were scored according to Kämper et al. (Kämper et al. 2006). Consistence of replicates
393 was tested using a chi-squared test and p-values were computed using 1,000,000 permutations. As
394 no significant difference between replicates was observed (p-value = 0.347 for the wildtype and p-
395 value = 0.829 for the deletion strain), observation were pooled between all replicates for each strain
396 before being compared.

397 ## Blast searches and gene alignment

398 We performed BlastN and BlastP (Altschul et al. 1990) searches using the (translated)
399 sequence of *UMAG_11064* as a query using NCBI online blast tools. The non-redundant nucleotide
400 and protein sequence databases were selected for BlastN and BlastP, respectively. Results were
401 further processed with scripts using the NCBIXML module from BioPython (Cock et al. 2009). The
402 Macse codon aligner (Ranwez et al. 2011) was used in order to infer the position of putative
403 frameshifts in the upstream region of *UMAG_11064*. The alignment was depicted using the
404 Boxshade software and was further manually annotated. The sequences of *U. maydis cox1* intron 6,
405 as well as *S. reilianum cox1* introns 1 and 2 were used as query and searched against the protein non
406 redundant database using NCBI BlastX, excluding environmental samples and model sequences.
407 The *cox1* genes from *U. maydis* and *S. reilianum* were aligned and pairwise similarity was
408 computed in non-overlapping 100 bp windows (Supplementary File S1). The gene structure,
409 synteny and local pairwise similarity was depicted using the genoPlotR package for R (Guy et al.
410 2010).

411 ## Phylogeny estimation, estimation of dN/dS ratios and tests of positive
412 selection

413 The nucleotide sequence of *UMAG_11064*, the first intron of the *cox1* gene of *S.*
414 *reilianum*, and the eight non-redundant, most similar matches from BlastP (Table S2) were aligned
415 using the Macse codon aligner (Ranwez et al. 2011) together with the unannotated but similar
416 nucleotide sequences from *S. scitamineum*, *U. bromivora*, *T. indica* and *T. walkiri*, using the NCBI
417 codon translation table 4 "mitochondrial mold". Columns in the alignment were manually selected
418 to discard ambiguously aligned regions and a phylogeny was inferred using PhyML (Guindon et al.
419 2010) with a General Time Reversible (GTR) model of nucleotide evolution and a 4-classes discrete
420 gamma distribution of rates. The tree topology was inferred using the "best of nearest-neighbor-

421 interchange (NNI) and subtree-pruning-regrafting (SPR)" option, and 100 non-parametric bootstrap
422 replicated were obtained. The final tree was rooted using the midpoint method. Analyses were
423 performed using the Seaview software (Gouy et al. 2010). For the positive selection analysis, the *S.*
424 *scitamineum* and *U. bromivera* sequences were discarded as they contained multiple frameshifts. A
425 phylogenetic tree was estimated using PhyML from the remaining species after translation using a
426 Le and Gascuel model of protein evolution (Le and Gascuel 2008), and other parameters as for the
427 nucleotide model. Nodes with bootstrap support values lower than 65% were collapsed. A branch
428 model of codon evolution was fitted on the alignment and the inferred phylogenetic tree using
429 PAML 4.9d (Yang 2007), keeping selected positions that may contain missing data. The F3X4
430 codon frequencies model was selected, and one dN/dS ratio was estimated per branch. A branch-site
431 model (Zhang et al. 2005) was fitted by specifying the branch leading to the *UMAG_11064* gene as
432 the "foreground" group, putatively evolving under positive selection. Test for selection was
433 performed as suggested in the PAML manual, comparing to a model where the omega2 parameter is
434 fixed to a value of 1. A similar test was conducted after excluding the two *Tilletia* sequences from
435 the "background" branches, as they were found to have each a branch with dN/dS > 1.

436 Amplification of the *UMAG_11064* regions in several *U. maydis* strains

437 Amplification of DNA fragments via polymerase chain reaction (PCR) was done using
438 the Phusion High Fidelity DNA_Polymerase (Thermo Fisher Scientific, Waltham, USA). The PCR
439 reactions were set up in a 20 µl reaction volume using DNA templates indicated in the respective
440 experiments and buffer recommended by the manufacturer containing a final concentration of 3%
441 DMSO. The PCR programs used are represented by the following scheme: Initial denaturation –
442 [denaturation – annealing – elongation] x number cycles – final elongation. *UMAG_11072* was
443 amplified with primers um11072_ORF_fw x um11072_ORF_rv using 98 °C/3 m - [98 °C/10 s – 65
444 °C/30 s - 72 °C/45 s] x 30 cycles - 72 °C/10 m. *UMAG_11064* was amplified with primers

445 um11064_ORF_fw x um11064_ORF_rv using 98 °C/3 m - [98 °C/10 s – 65 °C/30 s - 72 °C/45 s] x
446 30 cycles - 72 °C/10 m. The *cox1* exons 1+2 were amplified with primers cox1_ex1_rv x
447 cox1_ex2_fw using 98 °C/3 m - [98 °C/10 s – 63 °C/30 s - 72 °C/90 s] x 33 cycles - 72 °C/10 m.
448 cox1 exon 7 was amplified with primers cox1_ex7_fw X cox1_ex7_rv using 98 °C/3 m - [98 °C/10
449 s – 67 °C/30 s - 72 °C/60 s] x 30 cycles - 72 °C/10 m. Parts of the genomic region containing
450 *UMAG_11064*, *UMAG_11065* and *UMAG_11066* were amplified with primer pairs um11064_fw1 x
451 um11064_rv1, um11064_fw1 x um11064_rv2; and um11064_ fw2 x um11064_rv2 using 98 °C/3 m
452 - [98 °C/10 s – 65 °C/30 s - 72 °C/150 s] x 32 cycles - 72 °C/10 m. The list of all primer sequences
453 is provided in Supplementary Table S7. PCR results are shown in Figures S1 and S2.

454 History of the *UMAG_11065* family

455 The sequence of the *UMAG_11065* protein was used as a query for a search against
456 several smut fungi (*U. maydis*, *U. hordei*, *S. reilianum*, *S. scitamineum*, *Melanopsichum*
457 *pennsylvanicum*, *Pseudozyma flocculosa*) complete proteome using BlastP (Altschul et al. 1990).
458 The search finds 17 hits within the *U. maydis* genome with an E-value below 0.0001, as well as two
459 genes in *S. scitamineum* (*SPSC_04622* and *SPSC_05783*) and two genes in *P. flocculosa*
460 (*PFL1_06135* and *PFL1_02192*). Using NCBI BlastP, we found several sequences from *Fusarium*
461 *oxyparum* with high similarity. We selected the sequence *FOXG_04692* as a representative and
462 added it to the data set. The Guidance web server with the GUIDANCE2 algorithm was then used
463 to align the protein sequences and assess the quality of the resulting alignment. Default options
464 from the server were kept, selecting the MAFFT aligner (Katoh et al. 2002). Several sequences
465 appeared to be of shallow alignment quality and were discarded. The remaining sequences were
466 realigned using the same protocol. Four iterations were performed until the final alignment had a
467 quality good enough for phylogenetic inference. The final alignment contained 14 sequences and
468 had a global score of 0.79. These 14 alignable sequences contained 13 *U. maydis* sequences
469 (including *UMAG_11065*), and the *F. oxysporum* gene, other sequences from smut genomes were

470 too divergent to be unambiguously aligned. Using Guidance, we further masked columns in the
471 alignment with a score below 0.93 (a maximum of one position out of 14 in the column was
472 allowed to be uncertain).

473 A phylogenetic analysis was conducted using the program Seaview 4 (Gouy et al. 2010).
474 First, a site selection was performed in order to filter regions with too many gaps, leaving 506 sites.
475 Second, a phylogenetic tree was built using PhyML within Seaview (Guindon et al. 2010) (Le and
476 Gascuel protein substitution model (Le and Gascuel 2008) with a four-classes discretized gamma
477 distribution of rates, the best tree of Nearest Neigbour Interchange (NNI) and Subtree Pruning and
478 Regrafting (SPR) topological searches was kept). Support values were computed using the
479 approximate likelihood ratio test (aLRT) method (Anisimova and Gascuel 2006).

480 A test for positive selection was conducted using a combination of branch and branch-site
481 models using PAML (Yang 2007). The final GUIDANCE alignment was used, realigned using the
482 Macse codon aligner (Ranwez et al. 2011), and ambiguously aligned sites and shorter sequences
483 were manually filtered. The final alignment contained the following sequences: *UMAG_03394*,
484 *UMAG_11065*, *UMAG_04486*, *UMAG_06506*, *UMAG_04094*, *UMAG_10585*, *UMAG_06474*,
485 *UMAG_10980*, *UMAG_05977*, *FOXG_04692*. We used the PhyML software with the same options
486 as described above to reconstruct a phylogenetic tree with this subset of sequences. The branch
487 toward the *UMAG_11065* gene was used as a foreground group in the branch site model.

488 Gene expression

489 RNASeq normalized expression counts for the *UMAG_11064* and *UMAG_11065*, as well
490 as of neighbouring genes and paralogs elsewhere in the genome, were extracted from the Gene
491 Expression Omnibus data set GSE103876 (Lanver et al. 2018). Gene clustering based on expression
492 profiles was conducted using a hierarchical clustering with an average linkage on a Canberra
493 distance, suitable for expression counts, as implemented in the 'dist' and 'hclust' functions in R (R
494 Core Team 2018). The resulting clustering tree was converted to a distance matrix and compared to

495 the inferred phylogeny of the genes using a Mantel permutation test, as implemented in the 'ape'
496 package for R (Paradis et al. 2004). Differences in expression between time points were assessed by
497 fitting the linear model "expression ~ time * gene", testing the effect of time while controlling for
498 interaction with the "gene" variable. Residuals were normalized using a Box-Cox transform as
499 implemented in the MASS package for R. Tukey's posthoc comparisons were conducted on the
500 resulting model, allowing for a 5% false discovery rate.

501 *Acknowledgments*

502 We thank all members of our groups for stimulating discussions. We are grateful to
503 Georgiana May and Octavio Paredes-López for providing field isolates of *U. maydis* from the US
504 and Mexico, respectively. We acknowledge the generous support by the Max Planck Society.

505 *Conflict of interest disclosure*

506 The authors of this study declare that they have no financial conflict of interest with the
507 content of this article.

508 *References*

Altschul SF, Gish W, Miller W, Myers EW, Lipman DJ. 1990. Basic local alignment search tool. *J Mol Biol* **215**: 403–410.

Anisimova M, Gascuel O. 2006. Approximate likelihood-ratio test for branches: A fast, accurate, and powerful alternative. *Syst Biol* **55**: 539–552.

Ast J, Stiebler AC, Freitag J, Bölker M. 2013. Dual targeting of peroxisomal proteins. *Front Physiol* **4**: 297.

Banuett F, Herskowitz I. 1989. Different a alleles of *Ustilago maydis* are necessary for maintenance of filamentous growth but not for meiosis. *Proc Natl Acad Sci U S A* **86**: 5878–5882.

Barzel A, Obolski U, Gogarten JP, Kupiec M, Hadany L. 2011. Home and away- the evolutionary dynamics of homing endonucleases. *BMC Evol Biol* **11**: 324.

Basse CW. 2010. Mitochondrial inheritance in fungi. *Curr Opin Microbiol* **13**: 712–719.

Belfort M, Roberts RJ. 1997. Homing endonucleases: keeping the house in order. *Nucleic Acids Res*

25: 3379–3388.

Boidin J. 1986. Intercompatibility and the species concept in the saprobic basidiomycotina. *Mycotaxon* **XXVI**: 319–336.

Charif D, Thioulouse J, Lobry JR, Perrière G. 2005. Online synonymous codon usage analyses with the ade4 and seqinR packages. *Bioinforma Oxf Engl* **21**: 545–547.

Chevalier BS, Stoddard BL. 2001. Homing endonucleases: structural and functional insight into the catalysts of intron/intein mobility. *Nucleic Acids Res* **29**: 3757–3774.

Cho Y, Qiu Y-L, Kuhlman P, Palmer JD. 1998. Explosive invasion of plant mitochondria by a group I intron. *Proc Natl Acad Sci* **95**: 14244–14249.

Christianson TW, Sikorski RS, Dante M, Shero JH, Hieter P. 1992. Multifunctional yeast high-copy-number shuttle vectors. *Gene* **110**: 119–122.

Cock PJA, Antao T, Chang JT, Chapman BA, Cox CJ, Dalke A, Friedberg I, Hamelryck T, Kauff F, Wilczynski B, et al. 2009. Biopython: freely available Python tools for computational molecular biology and bioinformatics. *Bioinforma Oxf Engl* **25**: 1422–1423.

Derbyshire V, Kowalski JC, Dansereau JT, Hauer CR, Belfort M. 1997. Two-domain structure of the td intron-encoded endonuclease I-TevI correlates with the two-domain configuration of the homing site. *J Mol Biol* **265**: 494–506.

Djamei A, Kahmann R. 2012. *Ustilago maydis*: dissecting the molecular interface between pathogen and plant. *PLoS Pathog* **8**: e1002955.

Dong S, Raffaele S, Kamoun S. 2015. The two-speed genomes of filamentous pathogens: waltz with plants. *Curr Opin Genet Dev* **35**: 57–65.

Dujon B, Belfort M, Butow RA, Jacq C, Lemieux C, Perlman PS, Vogt VM. 1989. Mobile introns: definition of terms and recommended nomenclature. *Gene* **82**: 115–118.

Dunin-Horkawicz S, Feder M, Bujnicki JM. 2006. Phylogenomic analysis of the GIY-YIG nuclease superfamily. *BMC Genomics* **7**: 98.

Dutheil JY, Mannhaupt G, Schweizer G, Sieber CMK, Münsterkötter M, Güldener U, Schirawski J, Kahmann R. 2016. A Tale of Genome Compartmentalization: The Evolution of Virulence Clusters in Smut Fungi. *Genome Biol Evol* **8**: 681–704.

Eyre-Walker A, Keightley PD. 2007. The distribution of fitness effects of new mutations. *Nat Rev Genet* **8**: 610–618.

Férandon C, Moukha S, Callac P, Benedetto J-P, Castroviejo M, Barroso G. 2010. The Agaricus bisporus cox1 Gene: The Longest Mitochondrial Gene and the Largest Reservoir of Mitochondrial Group I Introns. *PLoS ONE* **5**. http://www.ncbi.nlm.nih.gov/pmc/articles/PMC2987802/ (Accessed December 19, 2012).

Fischer C. 1957. *Biology and Control of Smut Fungi*. John Wiley & Sons Canada, Limited.

Fuentes I, Karcher D, Bock R. 2012. Experimental reconstruction of the functional transfer of

intron-containing plastid genes to the nucleus. *Curr Biol CB* **22**: 763–771.

Fukami H, Chen CA, Chiou C-Y, Knowlton N. 2007. Novel group I introns encoding a putative homing endonuclease in the mitochondrial cox1 gene of Scleractinian corals. *J Mol Evol* **64**: 591–600.

Gladyshev E. 2017. Repeat-Induced Point Mutation and Other Genome Defense Mechanisms in Fungi. *Microbiol Spectr* **5**.

Goddard MR, Burt A. 1999. Recurrent invasion and extinction of a selfish gene. *Proc Natl Acad Sci U S A* **96**: 13880–13885.

Gogarten JP, Hilario E. 2006. Inteins, introns, and homing endonucleases: recent revelations about the life cycle of parasitic genetic elements. *BMC Evol Biol* **6**: 94.

Gouy M, Guindon S, Gascuel O. 2010. SeaView version 4: A multiplatform graphical user interface for sequence alignment and phylogenetic tree building. *Mol Biol Evol* **27**: 221–224.

Grandaubert J, Lowe RGT, Soyer JL, Schoch CL, Van de Wouw AP, Fudal I, Robbertse B, Lapalu N, Links MG, Ollivier B, et al. 2014. Transposable element-assisted evolution and adaptation to host plant within the Leptosphaeria maculans-Leptosphaeria biglobosa species complex of fungal pathogens. *BMC Genomics* **15**: 891.

Guindon S, Dufayard J-F, Lefort V, Anisimova M, Hordijk W, Gascuel O. 2010. New algorithms and methods to estimate maximum-likelihood phylogenies: assessing the performance of PhyML 3.0. *Syst Biol* **59**: 307–321.

Guy L, Kultima JR, Andersson SGE. 2010. genoPlotR: comparative gene and genome visualization in R. *Bioinforma Oxf Engl* **26**: 2334–2335.

Jalalzadeh B, Saré IC, Férandon C, Callac P, Farsi M, Savoie J-M, Barroso G. 2015. The intraspecific variability of mitochondrial genes of Agaricus bisporus reveals an extensive group I intron mobility combined with low nucleotide substitution rates. *Curr Genet* **61**: 87–102.

Kaessmann H. 2010. Origins, evolution, and phenotypic impact of new genes. *Genome Res* **20**: 1313–1326.

Kämper J. 2004. A PCR-based system for highly efficient generation of gene replacement mutants in *Ustilago maydis*. *Mol Genet Genomics MGG* **271**: 103–110.

Kämper J, Kahmann R, Bölker M, Ma L-J, Brefort T, Saville BJ, Banuett F, Kronstad JW, Gold SE, Müller O, et al. 2006. Insights from the genome of the biotrophic fungal plant pathogen *Ustilago maydis*. *Nature* **444**: 97–101.

Katoh K, Misawa K, Kuma K, Miyata T. 2002. MAFFT: a novel method for rapid multiple sequence alignment based on fast Fourier transform. *Nucleic Acids Res* **30**: 3059–3066.

Khrunyk Y, Münch K, Schipper K, Lupas AN, Kahmann R. 2010. The use of FLP-mediated recombination for the functional analysis of an effector gene family in the biotrophic smut fungus *Ustilago maydis*. *New Phytol* **187**: 957–968.

Kojic M, Holloman WK. 2012. Brh2 domain function distinguished by differential cellular responses to DNA damage and replication stress. *Mol Microbiol* **83**: 351–361.

Kondrashov FA, Kondrashov AS. 2010. Measurements of spontaneous rates of mutations in the recent past and the near future. *Philos Trans R Soc Lond B Biol Sci* **365**: 1169–1176.

Krombach S, Reissmann S, Kreibich S, Bochen F, Kahmann R. 2018. Virulence function of the *Ustilago maydis* sterol carrier protein 2. *New Phytol* **220**: 553–566.

Lambowitz AM, Belfort M. 1993. Introns as mobile genetic elements. *Annu Rev Biochem* **62**: 587–622.

Lanver D, Müller AN, Happel P, Schweizer G, Haas FB, Franitza M, Pellegrin C, Reissmann S, Altmüller J, Rensing SA, et al. 2018. The Biotrophic Development of *Ustilago maydis* Studied by RNA-Seq Analysis. *Plant Cell* **30**: 300–323.

Laurie JD, Ali S, Linning R, Mannhaupt G, Wong P, Güldener U, Münsterkötter M, Moore R, Kahmann R, Bakkeren G, et al. 2012. Genome comparison of barley and maize smut fungi reveals targeted loss of RNA silencing components and species-specific presence of transposable elements. *Plant Cell* **24**: 1733–1745.

Le SQ, Gascuel O. 2008. An improved general amino acid replacement matrix. *Mol Biol Evol* **25**: 1307–1320.

Lloyd AH, Timmis JN. 2011. The origin and characterization of new nuclear genes originating from a cytoplasmic organellar genome. *Mol Biol Evol* **28**: 2019–2028.

Louis EJ, Haber JE. 1991. Evolutionarily recent transfer of a group I mitochondrial intron to telomere regions in Saccharomyces cerevisiae. *Curr Genet* **20**: 411–415.

Lynch M. 2007. *The Origins of Genome Architecture*. Sinauer Associates.

Lynch M, Sung W, Morris K, Coffey N, Landry CR, Dopman EB, Dickinson WJ, Okamoto K, Kulkarni S, Hartl DL, et al. 2008. A genome-wide view of the spectrum of spontaneous mutations in yeast. *Proc Natl Acad Sci U S A* **105**: 9272–9277.

Mewes HW, Ruepp A, Theis F, Rattei T, Walter M, Frishman D, Suhre K, Spannagl M, Mayer KFX, Stümpflen V, et al. 2011. MIPS: curated databases and comprehensive secondary data resources in 2010. *Nucleic Acids Res* **39**: D220-224.

Möller M, Stukenbrock EH. 2017. Evolution and genome architecture in fungal plant pathogens. *Nat Rev Microbiol* **15**: 756–771.

Munkacsi AB, Stoxen S, May G. 2008. *Ustilago maydis* populations tracked maize through domestication and cultivation in the Americas. *Proc Biol Sci* **275**: 1037–1046.

Ohta T. 2000. Evolution of gene families. *Gene* **259**: 45–52.

Paradis E, Claude J, Strimmer K. 2004. APE: Analyses of Phylogenetics and Evolution in R language. *Bioinforma Oxf Engl* **20**: 289–290.

Perrière G, Thioulouse J. 2002. Use and misuse of correspondence analysis in codon usage studies.

Nucleic Acids Res **30**: 4548–4555.

Pogoda CS, Keepers KG, Nadiadi AY, Bailey DW, Lendemer JC, Tripp EA, Kane NC. 2019. Genome streamlining via complete loss of introns has occurred multiple times in lichenized fungal mitochondria. *Ecol Evol* **9**: 4245–4263.

R Core Team. 2018. *R: A Language and Environment for Statistical Computing*. R Foundation for Statistical Computing https://www.R-project.org/.

Ranwez V, Harispe S, Delsuc F, Douzery EJP. 2011. MACSE: Multiple Alignment of Coding SEquences accounting for frameshifts and stop codons. *PloS One* **6**: e22594.

Sánchez-Alonso P, Guzmán P. 1998. Organization of chromosome ends in *Ustilago maydis*. RecQ-like helicase motifs at telomeric regions. *Genetics* **148**: 1043–1054.

Sanchez-Puerta MV, Abbona CC, Zhuo S, Tepe EJ, Bohs L, Olmstead RG, Palmer JD. 2011. Multiple recent horizontal transfers of the cox1 intron in Solanaceae and extended co-conversion of flanking exons. *BMC Evol Biol* **11**: 277.

Sanchez-Puerta MV, Cho Y, Mower JP, Alverson AJ, Palmer JD. 2008. Frequent, phylogenetically local horizontal transfer of the cox1 group I Intron in flowering plant mitochondria. *Mol Biol Evol* **25**: 1762–1777.

Schirawski J, Mannhaupt G, Münch K, Brefort T, Schipper K, Doehlemann G, Di Stasio M, Rössel N, Mendoza-Mendoza A, Pester D, et al. 2010. Pathogenicity determinants in smut fungi revealed by genome comparison. *Science* **330**: 1546–1548.

Schuster A, Lopez JV, Becking LE, Kelly M, Pomponi SA, Wörheide G, Erpenbeck D, Cárdenas P. 2017. Evolution of group I introns in Porifera: new evidence for intron mobility and implications for DNA barcoding. *BMC Evol Biol* **17**: 82.

Schweizer G, Münch K, Mannhaupt G, Schirawski J, Kahmann R, Dutheil JY. 2018. Positively Selected Effector Genes and Their Contribution to Virulence in the Smut Fungus Sporisorium reilianum. *Genome Biol Evol* **10**: 629–645.

Singh DK, Ghosh AK, Croteau DL, Bohr VA. 2012. RecQ helicases in DNA double strand break repair and telomere maintenance. *Mutat Res* **736**: 15–24.

Steinberg G, Perez-Martin J. 2008. *Ustilago maydis*, a new fungal model system for cell biology. *Trends Cell Biol* **18**: 61–67.

Stoddard BL. 2005. Homing endonuclease structure and function. *Q Rev Biophys* **38**: 49–95.

Stone CL, Frederick RD, Tooley PW, Luster DG, Campos B, Winegar RA, Melcher U, Fletcher J, Blagden T. 2018. Annotation and analysis of the mitochondrial genome of Coniothyrium glycines, causal agent of red leaf blotch of soybean, reveals an abundance of homing endonucleases. *PLOS ONE* **13**: e0207062.

Sun CW, Callis J. 1993. Recent stable insertion of mitochondrial DNA into an Arabidopsis polyubiquitin gene by nonhomologous recombination. *Plant Cell* **5**: 97–107.

Thorsness PE, Weber ER. 1996. Escape and migration of nucleic acids between chloroplasts,

mitochondria, and the nucleus. *Int Rev Cytol* **165**: 207–234.

Valverde ME, Vandemark GJ, Martínez O, Paredes-López O. 2000. Genetic diversity of *Ustilago maydis* strains. *World J Microbiol Biotechnol* **16**: 49–55.

Volff J-N. 2006. Turning junk into gold: domestication of transposable elements and the creation of new genes in eukaryotes. *BioEssays News Rev Mol Cell Dev Biol* **28**: 913–922.

Vollmeister E, Schipper K, Baumann S, Haag C, Pohlmann T, Stock J, Feldbrügge M. 2012. Fungal development of the plant pathogen *Ustilago maydis*. *FEMS Microbiol Rev* **36**: 59–77.

Yang Z. 2007. PAML 4: phylogenetic analysis by maximum likelihood. *Mol Biol Evol* **24**: 1586–1591.

Zhang J, Nielsen R, Yang Z. 2005. Evaluation of an improved branch-site likelihood method for detecting positive selection at the molecular level. *Mol Biol Evol* **22**: 2472–2479.

509

Tables

Table 1: *UMAG_11065* paralogs in *U. maydis*, together with a homolog from *F. oxysporum* for comparison.

Gene	Chr / Scaffold / Contig	Start	End	Length of Chr / Scaffold / Contig	Number of introns	Length of protein	Relative position (1)	
UMAG_06476	Chromosome 3	1641500	1642057	1642070	0	185	99.98%	
UMAG_06474	Chromosome 3	1639598	1640203	1642070	0	201	99.87%	
UMAG_06506	Chromosome 7	951043	954234	957188	5	983	99.52%	
UMAG_10585	Chromosome 4	883585	884046	884984	0	153	99.87%	
UMAG_11065	Chromosome 9	1886	1263	733962	0	207	0.21%	
UMAG_03394	Chromosome 9	8836	5960	733962	0	958	1.01%	
UMAG_03869	Chromosome 10	687301	690648	692354	7	937	99.51%	
UMAG_04094	Chromosome 11	688670	689965	690620	0	431	99.81%	
UMAG_04486	Chromosome 14	605233	609089	611467	2	1175	99.30%	
UMAG_04308	Chromosome 14	1241	87	611467	0	384	0.11%	
UMAG_05977	Chromosome 20	523510	523884	523884	0	124	99.96%	(2)
UMAG_10980	Chromosome 22	398220	400499	403590	0	759	98.95%	
UMAG_12076	Contig 1.265	4214	5343	5343	0	376	89.43%	
FOXG_04692	Supercontig 2.5	9736	6398	2688632	0	1112	0.30%	

(1) Position reported to the length of the chromosome or contig.

(2) N-terminal fragment only.

Supplementary Table S1: Homology search results using *UMAG_11064* as a query on the NCBI non-redundant nucleotide database, using BlastN. All hits with an E-value lower than 1E-04 are included, alongside with corresponding alignment length and percentage of sequence identity.

Supplementary Table S2: Homology search results using *UMAG_11064* as a query on NCBI non-redundant protein database, using BlastP. All hits with an E-value lower than 1E-04 are included, alongside with corresponding alignment length and percentage of sequence identity.

Supplementary Table S3: Homology search results using *UMAG_11065* as a query on

526 NCBI non-redundant protein database, using BlastP. All hits with an E-value lower than 1E-04 are
527 included, alongside with corresponding alignment length and percentage of sequence identity.
528
529 **Supplementary Table S4:** Homology search results using *U. maydis cox1* intron 6 as a
530 query on a NCBI non-redundant protein database, using BlastX. All hits with an E-value lower than
531 1E-04 are included, alongside with corresponding alignment length and percentage of sequence
532 identity.
533
534 **Supplementary Table S5:** Homology search results using *S. reilianum cox1* intron 1 as a
535 query on a NCBI non-redundant protein database, using BlastX. All hits with an E-value lower than
536 1E-04 are included, alongside with corresponding alignment length and percentage of sequence
537 identity.
538
539 **Supplementary Table S6:** Homology search results using *S. reilianum cox1* intron 2 as a
540 query on a NCBI non-redundant protein database, using BlastX. All hits with an E-value lower than
541 1E-04 are included, alongside with corresponding alignment length and percentage of sequence
542 identity.
543
544 **Supplementary Table S7:** Primers used in this study.

545 *Figures*

546 **Figure 1:** Identification of the *UMAG_11064* gene. A) Within-group correspondence
547 analysis of *U. maydis* codon usage. Each gene is represented according to its coordinates along the
548 first two principal factors. The genomic origin of each gene is indicated by a cross for nuclear genes
549 and a dot for mitochondrial genes. B) Genomic context of the gene *UMAG_11064*. GC content in
550 300 bp windows sliding by 1 bp, and distribution of GC content in 300 bp windows of

551 mitochondrial genome of *U. maydis*. The dash line represents the median of the distribution.

552

553 **Figure 2:** Phylogeny of *UMAG_11064* and its homologous sequences. Maximum
554 likelihood tree inferred from nucleotides sequences. Node labels show bootstrap support values.
555 Discontinuous branches indicate that the corresponding sequence is pseudogenized, with multiple
556 frameshifts and insertions/deletions. Branch annotations show the minimum and maximum dN/dS
557 ratio (ω) estimated from 10 independent runs of the codeml program. The yellow triangle indicates
558 the supposed branch where the frameshift within the active domain of the ancestral HE occurred
559 (See Figure 3).

560

561 **Figure 3:** Alignment of *UMAG_11064* and its upstream sequence with intron 1 from the
562 *cox1* gene of *S. reilianum*, *T. indica* and *T. walkeri*, as well as the coding sequence of the *A.*
563 *bisporus* HE. Shading indicates the level of amino-acid conservation, showing conserved residues
564 (in black) and residues with similar biochemical properties (grayscale). Amino-acids noted as 'X'
565 have incomplete codons due to frameshifts. Highlighted exclamation marks denote inferred
566 frameshifts and '*' characters stop codons. The location of the active site of the HE (GVY-YVG) is
567 highlighted.

568

569 **Figure 4:** Intron structure of the *cox1* gene in *U. maydis* and *S. reilianum*. Annotated HEs
570 are indicated. Red boxes depict *cox1* exons, numbered from *e1* to *e9*. Introns are represented by
571 connecting lines and numbered *i1* to *i8*. Arrows within introns show LAGLIDADG (light blue) and
572 GIY-YIG HEs (pink). Dashed arrows correspond to HEGs inferred by blast search, while solid
573 arrows correspond to the annotation from the GenBank files. Piecewise sequence similarity between
574 *U. maydis* and *S. reilianum* is displayed with a color gradient.

575

576 **Figure 5:** Maximum likelihood phylogeny of *UMAG_11065 U. maydis* paralogs together
577 with the closest homolog from *F. oxysporum* (see Table 1). Nodes labels indicate support values as
578 percentage. Nodes with support values lower than 60% have been collapsed.
579
580 **Figure 6:** Genomic organisation around the *UMAG_11064* gene and structure of the *cox1*
581 gene in several *U. maydis* and *S. reilianum* strains, together with their phylogeny. Strains 521 and
582 518 are two strains resulting from the same spore from a field isolate from the U.S.A. SG200 is a
583 genetically engineered strain derived from a cross between the 518 and 521 strains. Strain 10-1 is
584 another field isolate from the U.S.A. Strains I2, O2, P2, S5 and T6 from field isolates from Mexico.
585
586 **Figure 7:** Patterns of gene expression for *UMAG_11064* and *UMAG_11065*, together
587 with neighboring and homologous genes. A) Gene expression profiles for genes in the chromosome
588 9 telomeric region (as depicted on Figure 1B). Straight lines represent three independent replicates,
589 while the blue curve depicts the smoothed conditional mean computed using the LOESS method. B)
590 Gene expression profiles for the *UMAG_11065* homologs (Figure 5). Legends as in A. C)
591 Clustering of the *UMAG_11065* homologs based on their averaged expression profile (see
592 Methods). Hpi: hours post-infection. Dpi: days post-infection.
593
594 **Figure 8:** Phenotype assessment of the double deletion strain. A) The simultaneous
595 deletion of *UMAG_11064* and *UMAG_11065* does not affect virulence. Maize seedlings were
596 infected with the indicated strains. Disease symptoms were scored at 12 dpi according to Kämper et
597 al. (Kämper et al. 2006) using the color code depicted on the right. Colors reflect the degree of
598 severity, from brown-red (severe) to light yellow (mild). Data represent mean of n = 3 biologically
599 independent experiments. Total numbers of infected plants are indicated above the respective
600 columns. B) Stress assay of the double deletion strain (Δ11064Δ11065), lacking both genes

601 *UMAG_11064* and *UMAG_11065*, compared to the parental SG200 strain. Assays were repeated at
602 least three times with comparable results.
603
604 **Figure 9:** Possible evolutionary scenario recapitulating the events leading to the
605 formation of the *UMAG_11064* and *UMAG_11065 U. maydis* genes. Importantly, each step in this
606 model may have occurred by genetic drift alone. Positive selection may have favored – but is not
607 required to explain – the spread of the nuclear and/or the loss of the mitochondrial HEGs.
608
609 **Supplementary Figure S1:** Amplification of the candidate region in the telomeric region
610 of chromosome 9. A) Genomic context based on the *U. maydis* reference genome, and location PCR
611 primers. B) PCR results with corresponding expected fragment sizes. Forward (fw) and reverse (rv)
612 primer sequences are provided in Table S7.
613
614 **Supplementary Figure S2:** Amplification of A) *UMAG_11064* , B) *UMAG_11072* and
615 *cox1* exons C) 1 and D) 7 in several *U. maydis* and *S. reilianum* strains. Forward (fw) and reverse
616 (rv) primer sequences are provided in Table S7. E) Summary table of the results. Plus and minus
617 signs indicate whether the corresponding gene could be amplified or not. Numbers indicate the size
618 of the amplified region in base pairs. Strains are labelled as in Figure 6.
619
620 **Supplementary Figure S3**: Verification of the deletion of *UMAG_11064* and
621 *UMAG_11065*. A) Schematic map of the genomic region containing *UMAG_11064* and
622 *UMAG_11065* in SG200 and SG200Δ11064Δ11065. Primers used to amplify the left and right
623 border sequences are indicated. B) DNA of SG200 and SG200Δ11064Δ11065 was cleaved with
624 Fsp1 and subjected tho southern blot analysis using a mixture of Probes 1 and 2 indicated in A). The
625 2.94 kb fragment is diagnostic for SG200 while the 4.19 kb fragment is diagnostic for the deletion

626 of *UMAG_11064* and *UMAG_11065*.

627

628 ***Supplementary file:***

629 **Supplementary File S1**: Scripts used to conduct the phylogenetic and statistical analyses,

630 As well as R code used to generate figures 1, 3, 4, 5 and 6.

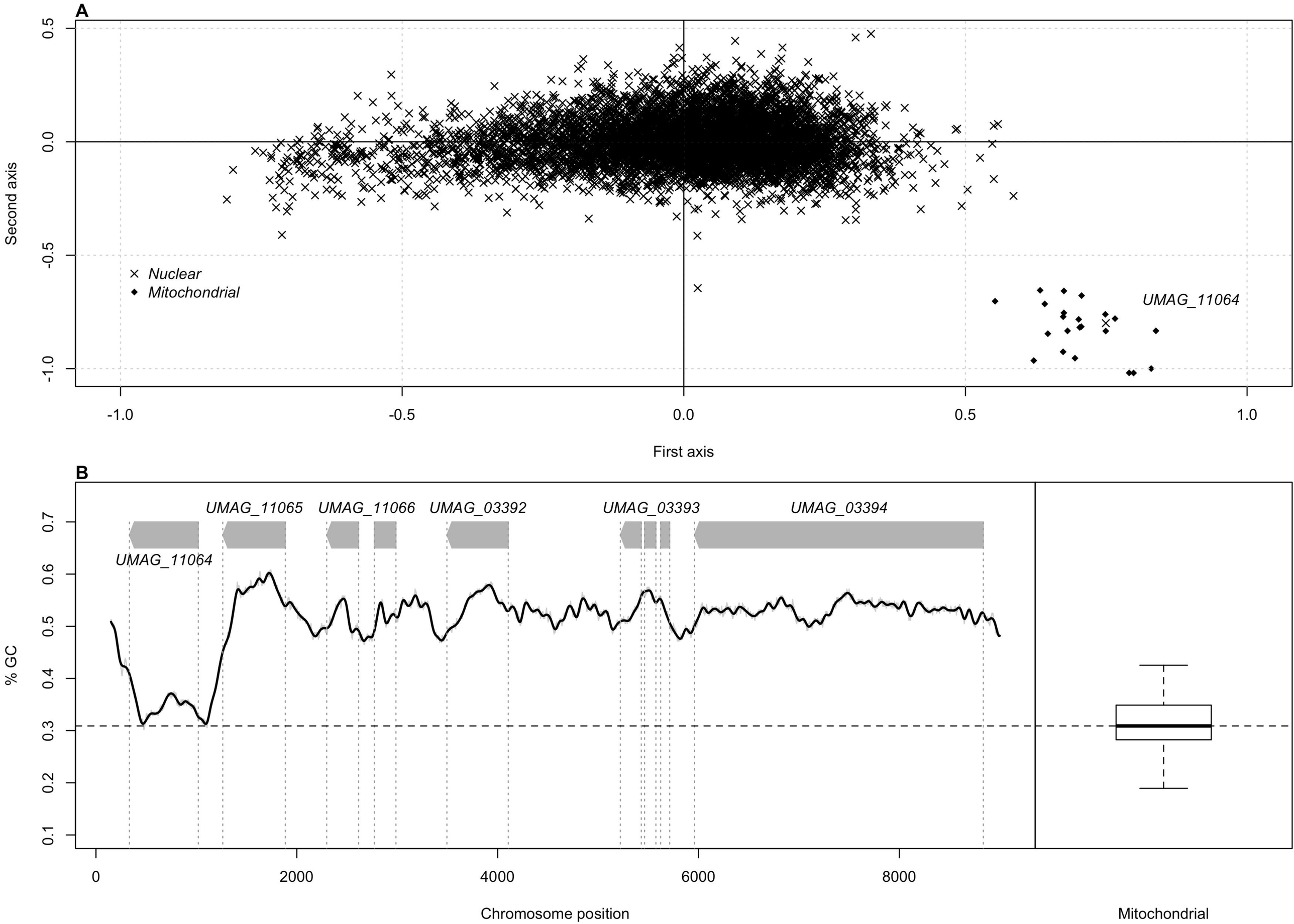
A
Second axis
First axis
Nuclear
Mitochondrial
UMAG_11064
B
% GC
UMAG_11064
UMAG_11065
UMAG_11066
UMAG_03392
UMAG_03393
UMAG_03394
Chromosome position
Mitochondrial

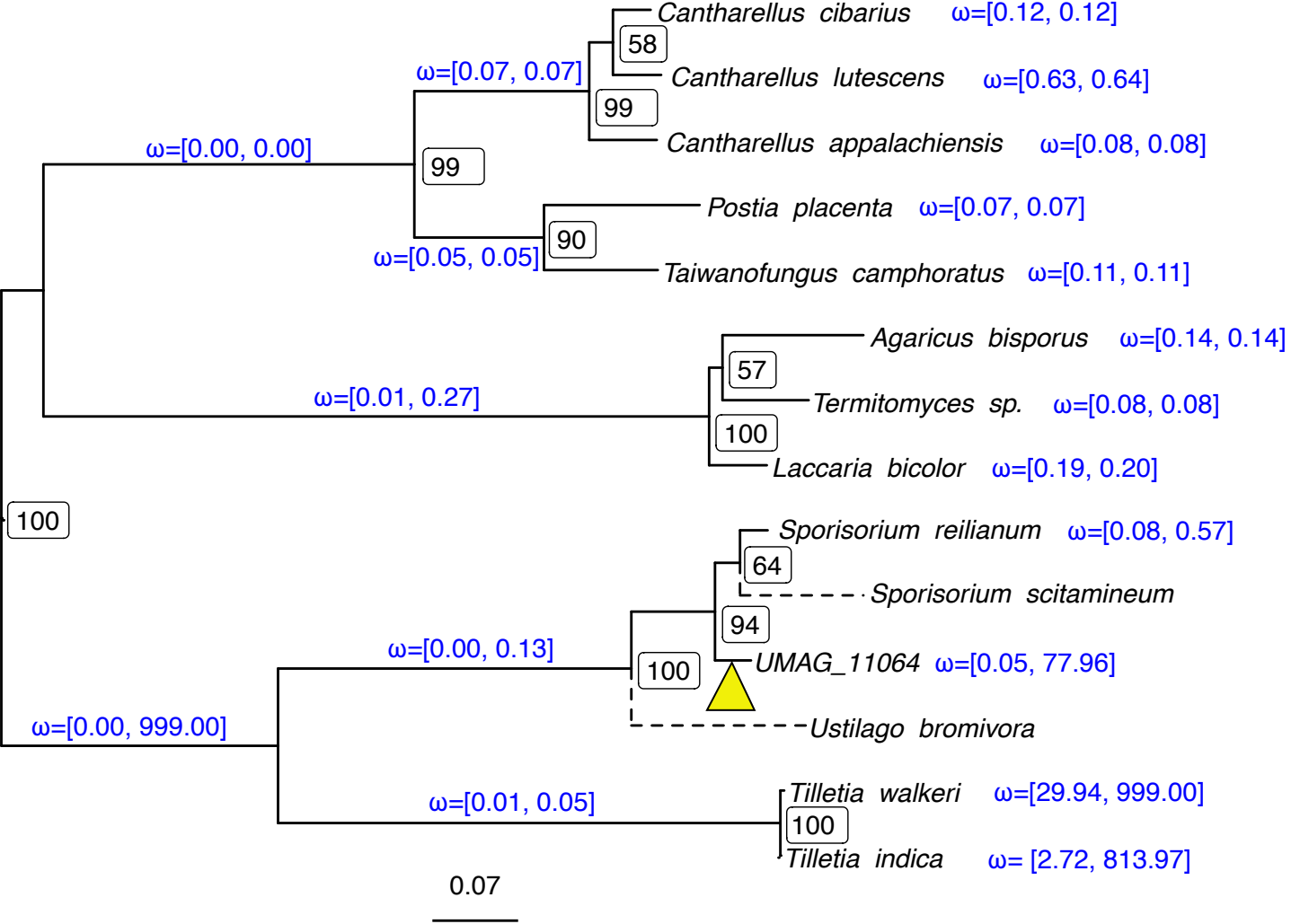
Cantharellus cibarius ω=[0.12, 0.12]
58
Cantharellus lutescens ω=[0.63, 0.64]
ω=[0.07, 0.07]
99
Cantharellus appalachiensis ω=[0.08, 0.08]
ω=[0.00, 0.00]
99
Postia placenta ω=[0.07, 0.07]
90
ω=[0.05, 0.05]
Taiwanofungus camphoratus ω=[0.11, 0.11]
Agaricus bisporus ω=[0.14, 0.14]
57
ω=[0.01, 0.27]
Termitomyces sp. ω=[0.08, 0.08]
100
Laccaria bicolor ω=[0.19, 0.20]
100
Sporisorium reilianum ω=[0.08, 0.57]
64
Sporisorium scitamineum
94
ω=[0.00, 0.13]
100
UMAG_11064 ω=[0.05, 77.96]
ω=[0.00, 999.00]
Ustilago bromivora
ω=[0.01, 0.05]
Tilletia walkeri ω=[29.94, 999.00]
100
Tilletia indica ω= [2.72, 813.97]
0.07

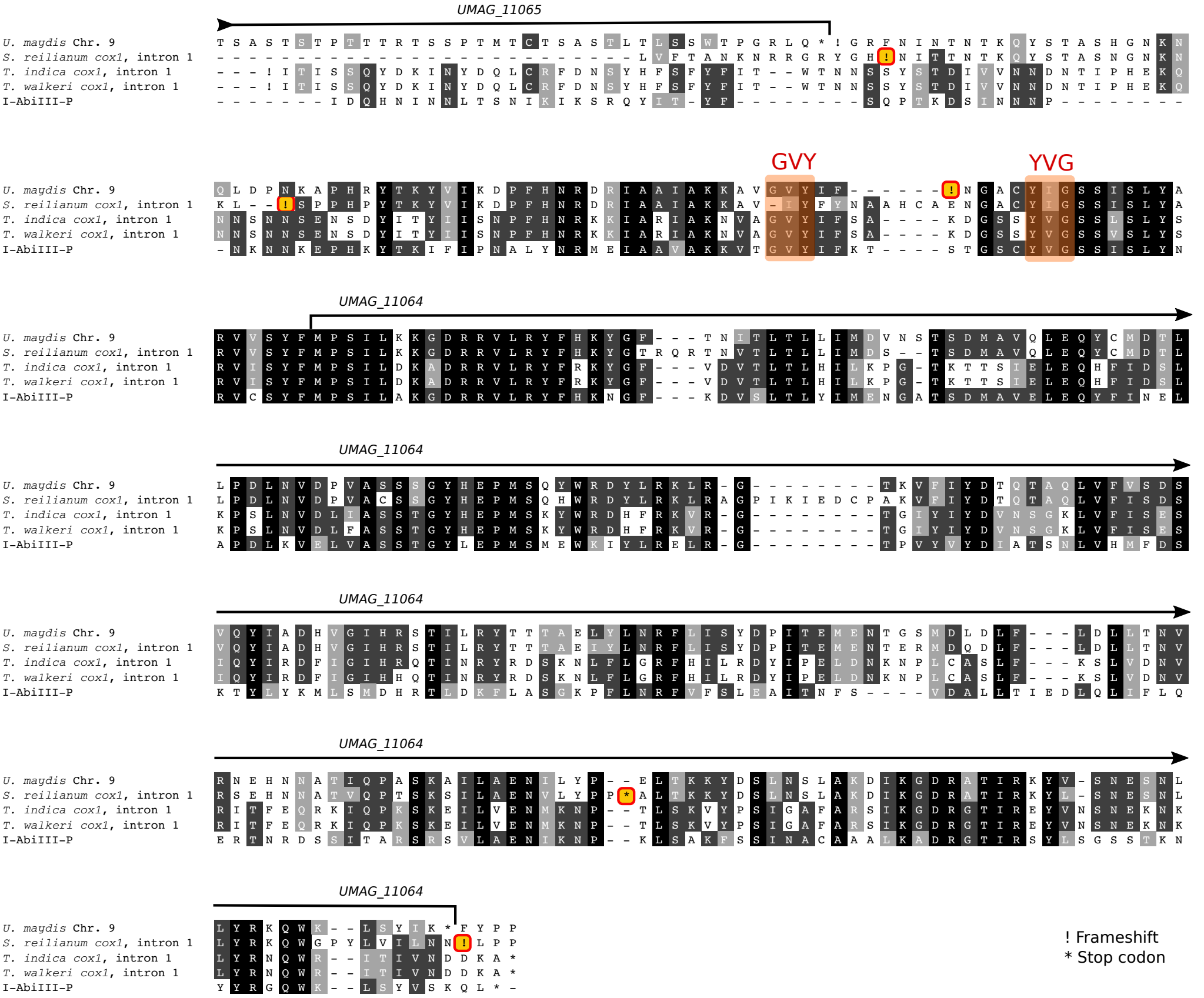
UMAG_11065
U. maydis Chr. 9
S. reilianum cox1, intron 1
T. indica cox1, intron 1
T. walkeri cox1, intron 1
I-AbiIII-P
GVY
YVG
UMAG_11064
UMAG_11064
UMAG_11064
UMAG_11064
! Frameshift
* Stop codon

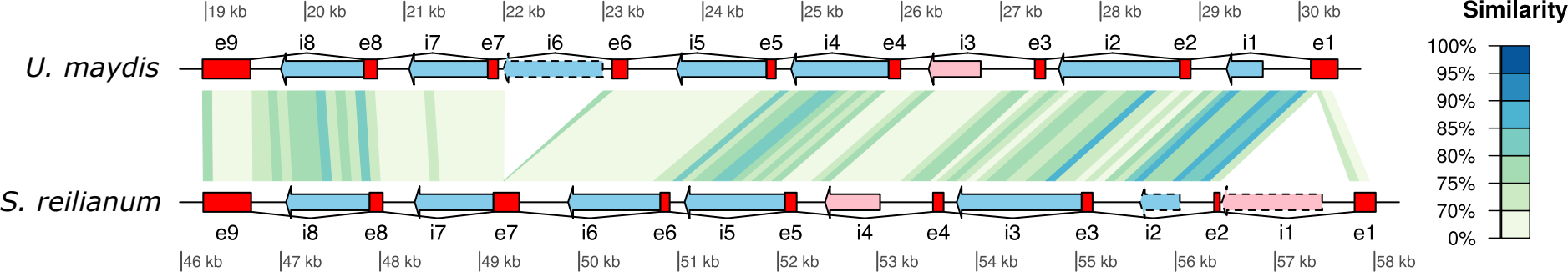
19 kb
20 kb
21 kb
22 kb
23 kb
24 kb
25 kb
26 kb
27 kb
28 kb
29 kb
30 kb
Similarity
U. maydis
e9
i8
e8
i7
e7
i6
e6
i5
e5
i4
e4
i3
e3
i2
e2
i1
e1
100%
95%
90%
85%
80%
75%
70%
0%
S. reilianum
e9
i8
e8
i7
e7
i6
e6
i5
e5
i4
e4
i3
e3
i2
e2
i1
e1
46 kb
47 kb
48 kb
49 kb
50 kb
51 kb
52 kb
53 kb
54 kb
55 kb
56 kb
57 kb
58 kb

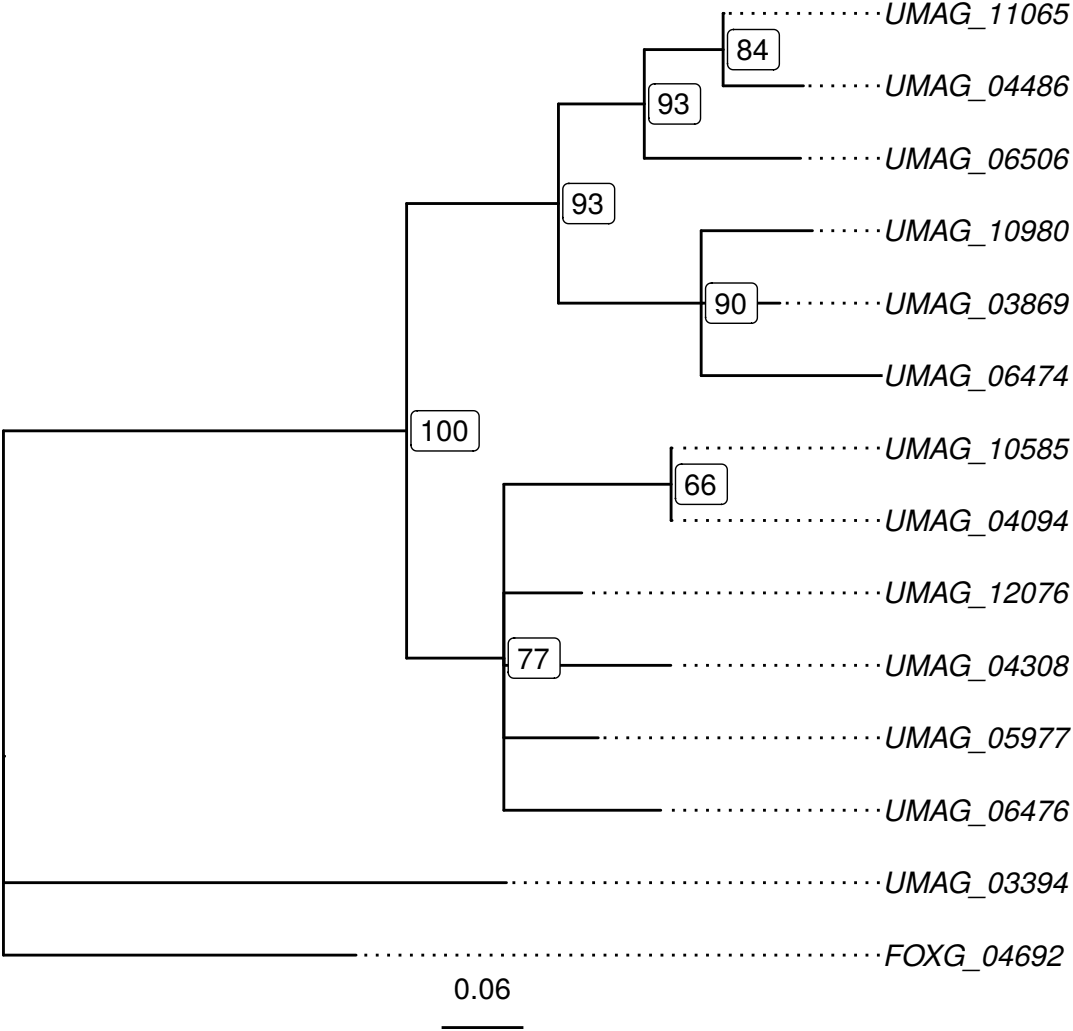
UMAG_11065
84
UMAG_04486
93
UMAG_06506
93
UMAG_10980
90
UMAG_03869
UMAG_06474
100
UMAG_10585
66
UMAG_04094
UMAG_12076
77
UMAG_04308
UMAG_05977
UMAG_06476
UMAG_03394
FOXG_04692
0.06

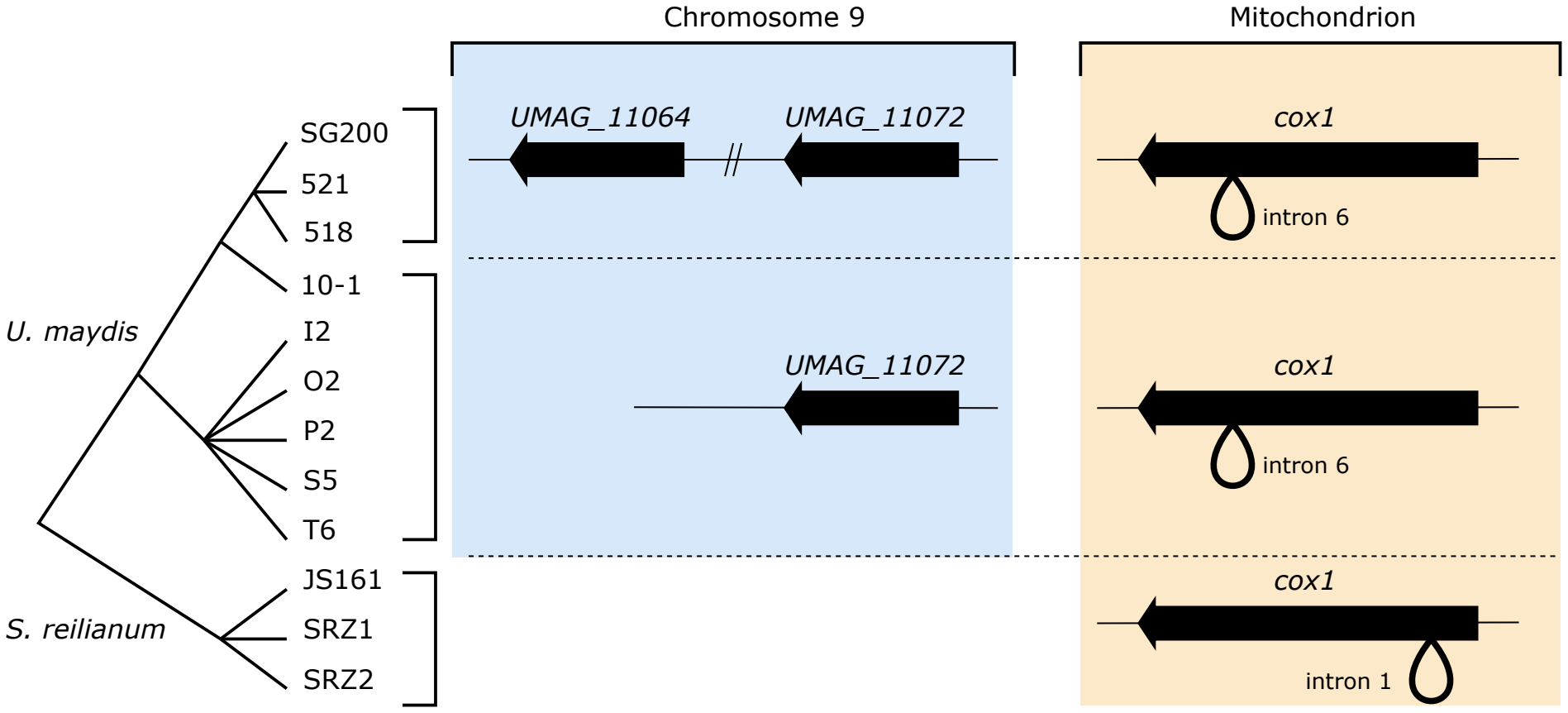
Chromosome 9
Mitochondrion
SG200
521
518
10-1
I2
O2
P2
S5
T6
JS161
SRZ1
SRZ2
U. maydis
S. reilianum
UMAG_11064
UMAG_11072
UMAG_11072
cox1
intron 6
cox1
intron 6
cox1
intron 1

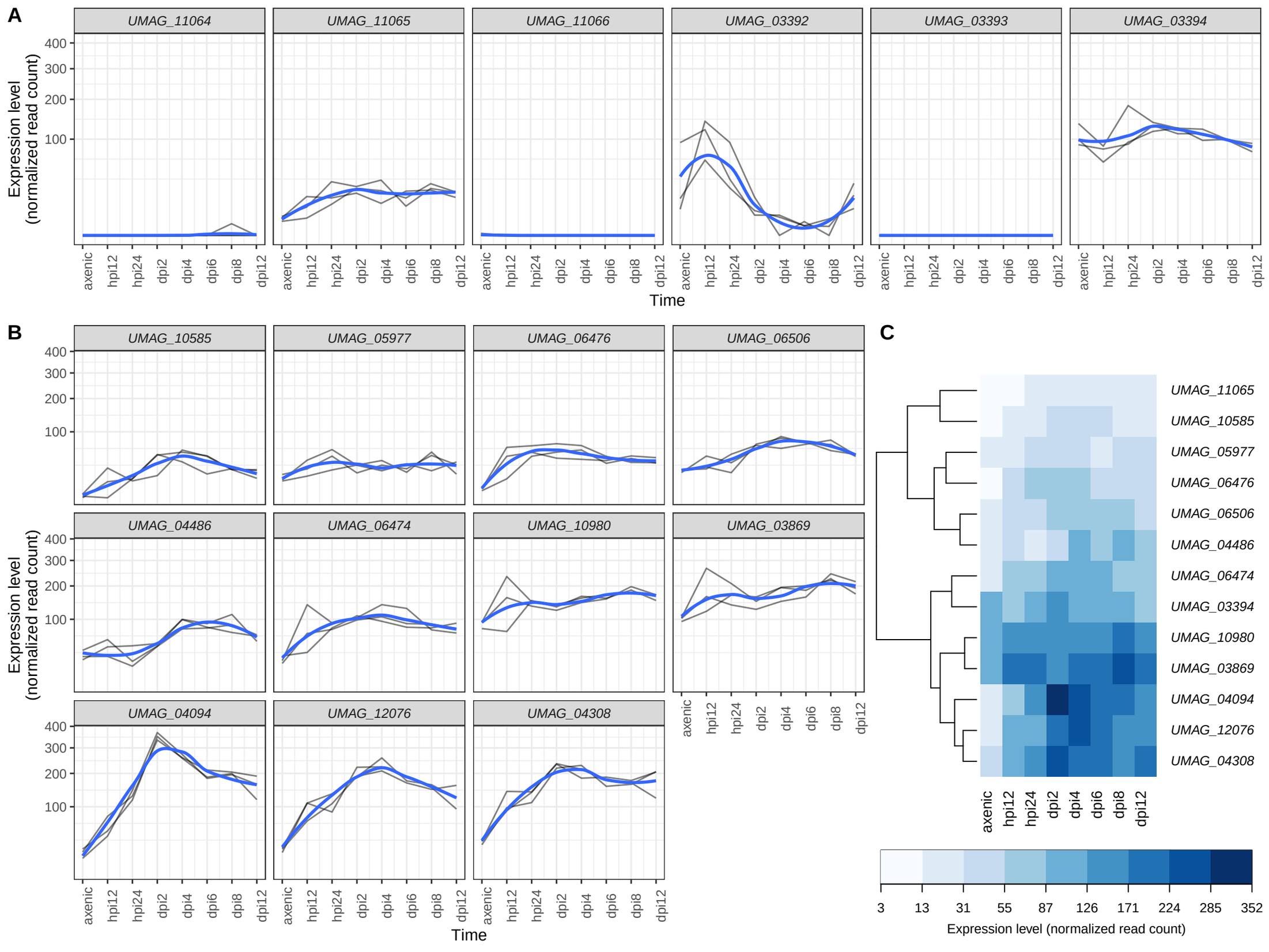
A
UMAG_11064
UMAG_11065
UMAG_11066
UMAG_03392
UMAG_03393
UMAG_03394
Expression level
(normalized read count)
400
300
200
100
axenic
hpi12
hpi24
dpi2
dpi4
dpi6
dpi8
dpi12
Time
B
UMAG_10585
UMAG_05977
UMAG_06476
UMAG_06506
UMAG_04486
UMAG_06474
UMAG_10980
UMAG_03869
UMAG_04094
UMAG_12076
UMAG_04308
C
UMAG_11065
UMAG_10585
UMAG_05977
UMAG_06476
UMAG_06506
UMAG_04486
UMAG_06474
UMAG_03394
UMAG_10980
UMAG_03869
UMAG_04094
UMAG_12076
UMAG_04308
3
13
31
55
87
126
171
224
285
352
Expression level (normalized read count)

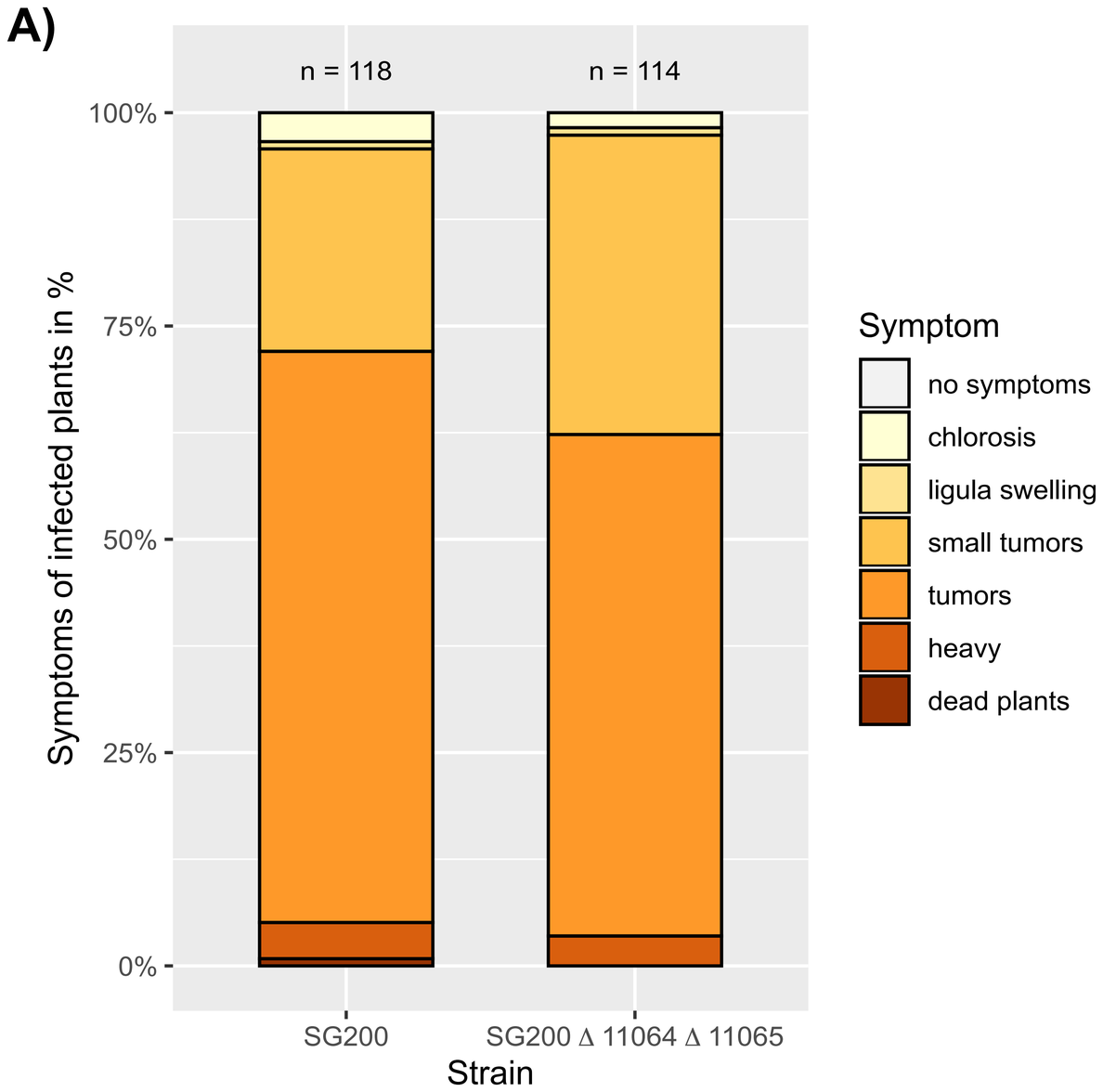
A)
n = 118
n = 114
100%
75%
50%
25%
0%
Symptoms of infected plants in %
SG200
SG200 Δ 11064 Δ 11065
Strain
Symptom
no symptoms
chlorosis
ligula swelling
small tumors
tumors
heavy
dead plants

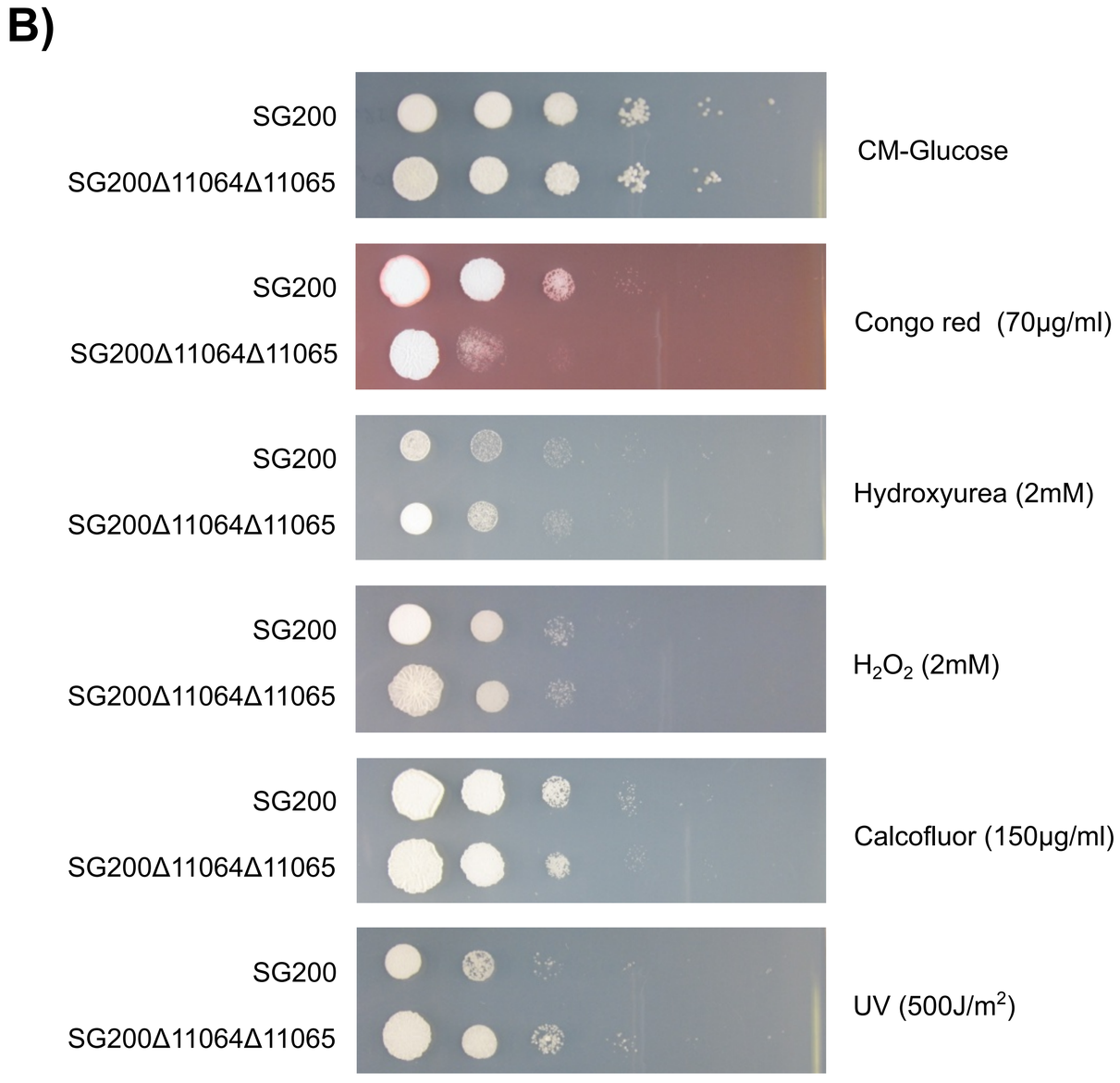
B)
SG200
SG200Δ11064Δ11065
CM-Glucose
Congo red (70µg/ml)
Hydroxyurea (2mM)
H_2O_2 (2mM)
Calcofluor (150µg/ml)
UV (500J/m^2)

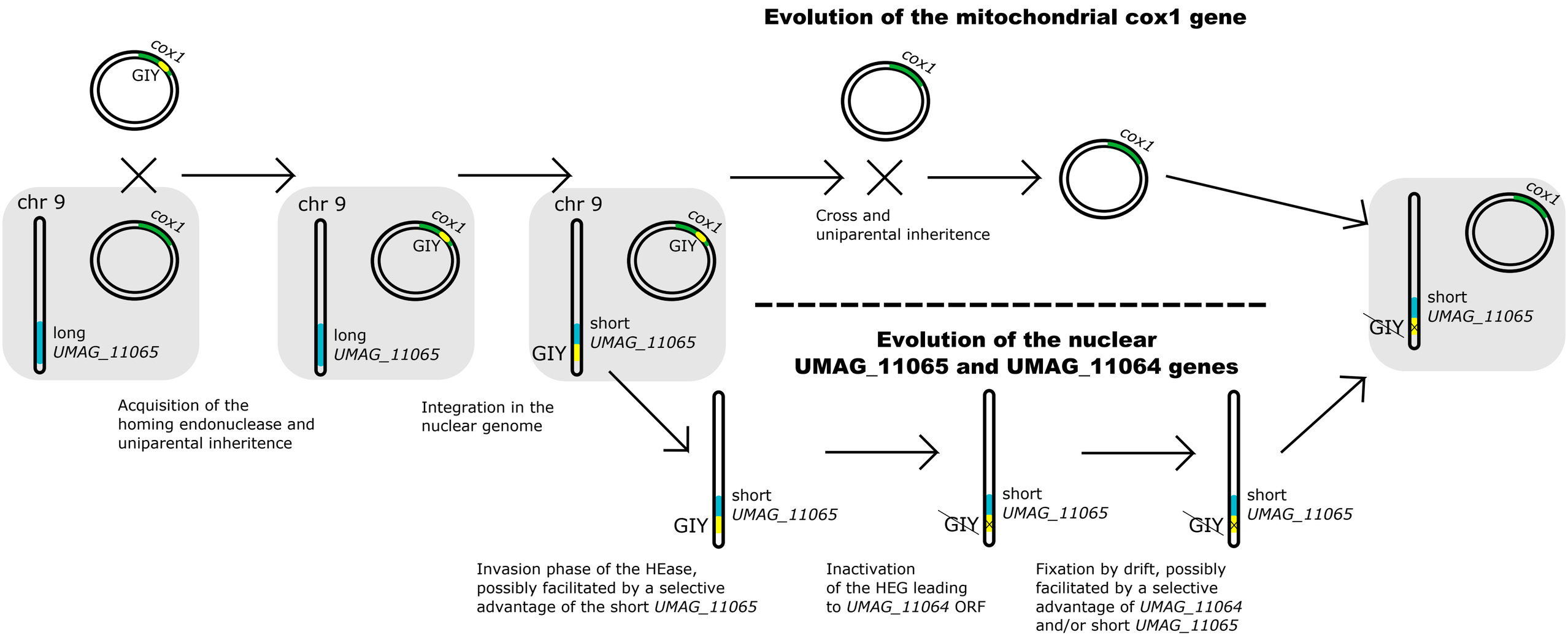
Evolution of the mitochondrial cox1 gene
cox1
GIY
chr 9
long
UMAG_11065
Acquisition of the homing endonuclease and uniparental inheritence
Integration in the nuclear genome
short
UMAG_11065
Cross and uniparental inheritence
Evolution of the nuclear UMAG_11065 and UMAG_11064 genes
Invasion phase of the HEase, possibly facilitated by a selective advantage of the short UMAG_11065
Inactivation of the HEG leading to UMAG_11064 ORF
Fixation by drift, possibly facilitated by a selective advantage of UMAG_11064 and/or short UMAG_11065